Journal of Structural Geology 58 (2014) 22–42

Contents lists available at ScienceDirect

Journal of Structural Geology

journal homepage: www.elsevier.com/locate/jsg

Lithological controls on the deformation mechanisms operating within carbonate-hosted faults during the seismic cycle☆

Rachael J. Bullock*, Nicola De Paola, Robert E. Holdsworth, João Trabucho-Alexandre

Rock Mechanics Laboratory, Earth Sciences Department, Durham University, South Road, Durham DH1 3LE, UK

ARTICLE INFO

Article history:
Received 5 July 2013
Received in revised form
7 October 2013
Accepted 20 October 2013
Available online 2 November 2013

Keywords:
Carbonate fault
Phyllosilicate
Fault zone heterogeneity
Seismic behaviour
Microstructure
Deformation mechanisms

ABSTRACT

A significant proportion of moderate-large earthquakes, plus aftershocks, nucleate within and propagate through upper-crustal carbonate-dominated sequences, where the effects of lithological variations on fault behaviour are poorly understood. The Gubbio fault is an active (1984, Ms = 5.2) normal fault in Italy, hosted in Mesozoic–Cenozoic limestones and interbedded marls. Fault core domains derived from limestone at the studied outcrop are characterised by fractures/hydrofractures and breccias and host a number of localised (<1.5 mm wide) principal slip zones (PSZs). The majority of displacement of up to 230 m is concentrated in these PSZs, which comprise cataclasites, gouges, and calcite veins. Degassing bubbles, 'quenched' calcite, and the transformation of smectite to illite, are also observed within PSZs, implying frictional heating and seismic slip. In contrast, marl-rich domains exhibit distributed shear planes bounding a continuous and pervasive foliation, defined by phyllosilicate-rich pressure-solution seams. Microstructures in the seams include folds/kinks of phyllosilicates and pressure shadows around clasts, consistent with aseismic fault creep. A model is proposed for the behaviour of lithologically complex carbonate-hosted faults during the seismic cycle, whereby limestone-dominated fault core domains behave in a predominantly seismic manner, whereas phyllosilicate-rich domains behave in a predominantly aseismic manner.

1. Introduction

The large-scale architecture of upper-crustal faults at <5 km depth comprises either a single high-strain fault core surrounded by a damage zone (e.g. Chester et al., 1993), or multiple high-strain cores, which bound lenses of damaged material (e.g. Faulkner et al., 2003). The differentiation between fault core and damage zone is generally based on the presence and spatial distribution of deformation products (Chester and Logan, 1986; Chester et al., 1993; Shipton et al., 2006). The fault core, which ranges from a few metres up to a few tens of metres wide, consists of cataclastically deformed fault rocks and typically contains one or more principal slip surfaces (PSSs) (Shipton et al., 2006; Faulkner et al., 2010). Damage zones, which are up to a few hundred metres in width, consist of fractured protolith rocks and smaller displacement subsidiary slip surfaces (Faulkner et al., 2010). The fault core is where most of the displacement is accommodated, and the deformation processes occurring here are the focus of the present paper.

Fault core architectures vary widely between faults and appear to be controlled, in part, by the composition of the protolith. Upper-crustal faults derived from carbonates (e.g. Agosta and Aydin, 2006; Micarelli et al., 2006; De Paola et al., 2008; Bastesen and Braathen, 2010; Molli et al., 2010; Smith et al., 2011a; Fondriest et al., 2012) and crystalline rocks (e.g. Chester and Chester, 1998; Wibberley and Shimamoto, 2003; Walker et al., 2013) tend to exhibit narrow fault cores that are less than a few metres in width, comprising cohesive and incohesive random-fabric fault rocks such as breccias, cataclasites and gouges (Sibson, 1977). The majority of the displacement within these fault cores is localised along discrete PSSs and within their associated principal slip zones (PSZs).

Numerous field studies of major seismogenic faults suggest that slip during individual earthquake events is localised along these PSZs, which are typically no more than a few cm thick (see Sibson, 2003, for a review). Notable examples include: the PSZ associated with the 1999 Mw 7.6 Chi Chi thrust earthquake in Taiwan, which has been estimated to be just 1 mm thick (Kuo et al., 2013); the Nojima fault, responsible for the 1995 M 7.2 Kobe earthquake in Japan, which contains several gouge and pseudotachylyte layers,

* Corresponding author. Tel.: +44 (0)191 3342300.
E-mail addresses: r.j.bullock@durham.ac.uk (R.J. Bullock), nicola.de-paola@durham.ac.uk (N. De Paola), r.e.holdsworth@durham.ac.uk (R.E. Holdsworth), joao.trabucho@durham.ac.uk (J. Trabucho-Alexandre).

0191-8141/$ – see front matter © 2013 The Authors. Published by Elsevier Ltd. All rights reserved.
http://dx.doi.org/10.1016/j.jsg.2013.10.008

each less than a few mm thick (Otsuki et al., 2003); and the PSZ responsible for the 2008 Ms 8.0 Wenchuan earthquake in China, which comprises a ~1 cm thick layer of fault gouge (Li et al., 2013). At the microscale, PSZs are often observed to contain sub-zones, which range from a few hundred microns to a few millimetres in width, composed of variably developed cataclasites and gouges and frequently displaying Riedel shear geometries (e.g. Power and Tullis, 1989; Otsuki et al., 2003; De Paola et al., 2008; Smith et al., 2011a; Fondriest et al., 2012).

In contrast, upper-crustal fault zones rich in phyllosilicates typically display much wider fault cores, often adhering to the multiple fault cores model. For example, the exhumed Carboneras fault in SE Spain has a fault core up to 1 km wide (Faulkner et al., 2003), which comprises numerous high-strain gouge zones of a few metres in thickness (Faulkner et al., 2003). Similarly, the SAFOD (San Andreas Fault Observatory at Depth) borehole core and field studies of the Median Tectonic Line in Japan have revealed several phyllosilicate-rich fault core strands, each >1 m wide (Zoback et al., 2010; Holdsworth et al., 2011; Jefferies et al., 2006). Rather than displacement being localised within PSZs, it is uniformly distributed within each gouge band; and rather than random-fabric fault rocks being the dominant deformation products, phyllosilicate-rich fault cores typically display a continuous, highly foliated fabric, though Riedel shear geometries are still conspicuous features (e.g. Rutter et al., 1986, 2012; Faulkner et al., 2003).

Consequently, in lithologically heterogeneous, upper-crustal fault zones, where crystalline/carbonate and phyllosilicate-rich protoliths are interlayered, we might expect to see a complex fault zone architecture with separate domains of localised and distributed deformation. This geometry has been documented along ancient, exhumed examples of presently inactive major strike-slip faults (e.g. the Carboneras fault zone, Faulkner et al., 2003), low-angle normal faults (e.g. the Zuccale fault in Central Italy, Collettini and Holdsworth, 2004; Smith et al., 2011b) and in accretionary complexes (e.g. the Chrystalls Beach Complex mélange, New Zealand, Fagereng and Sibson, 2010). Attention now is turning to active fault zones, in an attempt to understand how lithological heterogeneities within multi-layered sequences cut by a fault may affect not only the fault zone architecture, but also the seismic behaviour of the fault (e.g. Nemser and Cowan, 2009; Chiaraluce, 2012; Gratier et al., 2013; Tesei et al., 2013).

Quartzo-feldspathic and carbonate rocks typically have sliding friction coefficients in the Byerlee range of 0.6–0.85 (Byerlee, 1978) and experimentally exhibit slip-weakening and velocity-weakening behaviour (Logan et al., 1992; Beeler et al., 1996; Marone et al., 1990; Gu and Wong, 1994; Verberne et al., 2010; Collettini et al., 2011), which is necessary for earthquake nucleation and unstable stick-slip behaviour (Dieterich and Kilgore, 1994; Marone, 1998; Scholz, 1998). These lithologies also display dynamic-weakening behaviour during high-velocity rotary shear experiments (see Di Toro et al., 2011, for a review), with the coefficient of friction reducing to sub-Byerlee values (<0.2) at seismic slip velocities, facilitating earthquake propagation.

In contrast, many phyllosilicates (e.g. talc, smectites) are weak, particularly when wet, (sliding friction ≪0.3, e.g. Behnsen and Faulkner, 2012) and most types exhibit velocity-strengthening behaviour (e.g. Saffer et al., 2001; Saffer and Marone, 2003; Moore and Lockner, 2004, 2011; Ikari et al., 2007, 2009, 2011; Morrow et al., 2007; Tembe et al., 2010; Behnsen and Faulkner, 2012; Sone et al., 2012; Tesei et al., 2012). Velocity-strengthening behaviour does not favour earthquake nucleation and rock units displaying this behaviour are expected to act as barriers to earthquake propagation due to a positive stress drop (Scholz, 1998). Thus, upper-crustal fault rocks rich in weak phyllosilicate minerals are thought to deform predominantly aseismically by fault creep. For example, the creeping behaviour of faults such as the San Andreas is attributed to the presence of smectitic phyllosilicates in fault gouges (e.g. Carpenter et al., 2011; Lockner et al., 2011; Holdsworth et al., 2011).

Over the course of the seismic cycle, a fault may experience a broad spectrum of slip rates. These range from mm/yr, during the interseismic period, to mm/day-week during the pre-seismic (earthquake nucleation) and post-seismic (afterslip) periods and, then, to slip rates of m/s during earthquake propagation. It seems reasonable to hypothesise that lithological heterogeneities within the fault core will strongly influence which parts of a fault zone deform seismically or aseismically during the different seismic intervals. To further investigate this proposal, we document here the deformational and microstructural characteristics of the Gubbio normal fault (1984, Ms = 5.2) in the northern Apennines of Italy (Fig. 1a). This upper-crustal, seismically active fault deforms a succession of alternating limestone and cm-scale marl beds. Outcrop to microscale deformation features within the Gubbio fault zone have previously been studied by Bussolotto et al. (2007), who characterised the spatial and temporal relationships of structures in the fault zone, together with a determination of the P/T conditions and fluid behaviour during deformation. Here, we use a combination of microstructural (optical microscopy and field emission scanning electron microscopy, SEM) and mineralogical analyses (energy-dispersive X-ray spectroscopy, EDX, and X-ray diffraction, XRD) to study the dominant deformation mechanisms active within the fault core, and to assess the likely influence of lithology on deformation style. We use these findings to propose a conceptual model for the long- (inter- and post-seismic period) and short-term (coseismic) frictional behaviour of the fault zone, which can then be tested by future experimental work.

2. Geological setting

The northern Apennines of Italy have undergone NE–SW shortening since the middle Miocene, resulting in the development of a NE-verging fold and thrust belt (Barchi et al., 1998b). In the Gubbio area, this deformation is represented by the NW–SE striking Gubbio anticline (De Paola et al., 2006 and references therein). An upper Pliocene–Quaternary late-orogenic extensional regime is superimposed upon the folds and thrusts, forming a series of extensional basins bounded by NNW–SSE trending normal faults (Barchi et al., 1998a; Boncio and Lavecchia, 2000) (Fig. 1a). This extensional regime currently dominates the tectonics of the northern Apennines, although it has a relatively slow separation rate of 2–3 mm/yr (D'Agostino et al., 2009).

The Gubbio fault is an active segment of a 150 km long fault system known as the Umbria Fault System (Collettini et al., 2003). The surface trace is 22 km long, striking NW–SE (~N130°) (Figs. 1a and 2a). Seismic reflection data suggest that it has a listric profile at depth, with average dips of ~60–70° to the SW at the surface, decreasing to 10–15° at ~6 km, where it reactivates a pre-existing thrust fault (Mirabella et al., 2004) (Fig. 1a). At the surface, the fault juxtaposes Jurassic-Oligocene carbonates, belonging to the Umbria–Marche succession, in the footwall against Quaternary fluvio-lacustrine deposits, of the Gubbio Basin, in the hangingwall (Collettini et al., 2003; Bussolotto et al., 2007) (Fig. 1b).

A maximum displacement of 3.2 km at the centre of the Gubbio Basin was estimated by Collettini et al. (2003), which accumulated during multiple tectonic phases. Historical and instrumental records of moderate-large earthquakes occurring on the Gubbio fault are limited, since no permanent station coverage exists (Collettini et al., 2003; Pucci et al., 2003). However in 1984, the Gubbio area experienced an Ms 5.2 (Haessler et al., 1988) earthquake, located ~10 km south of the town of Gubbio at 7 km depth (ISC, 2001), and

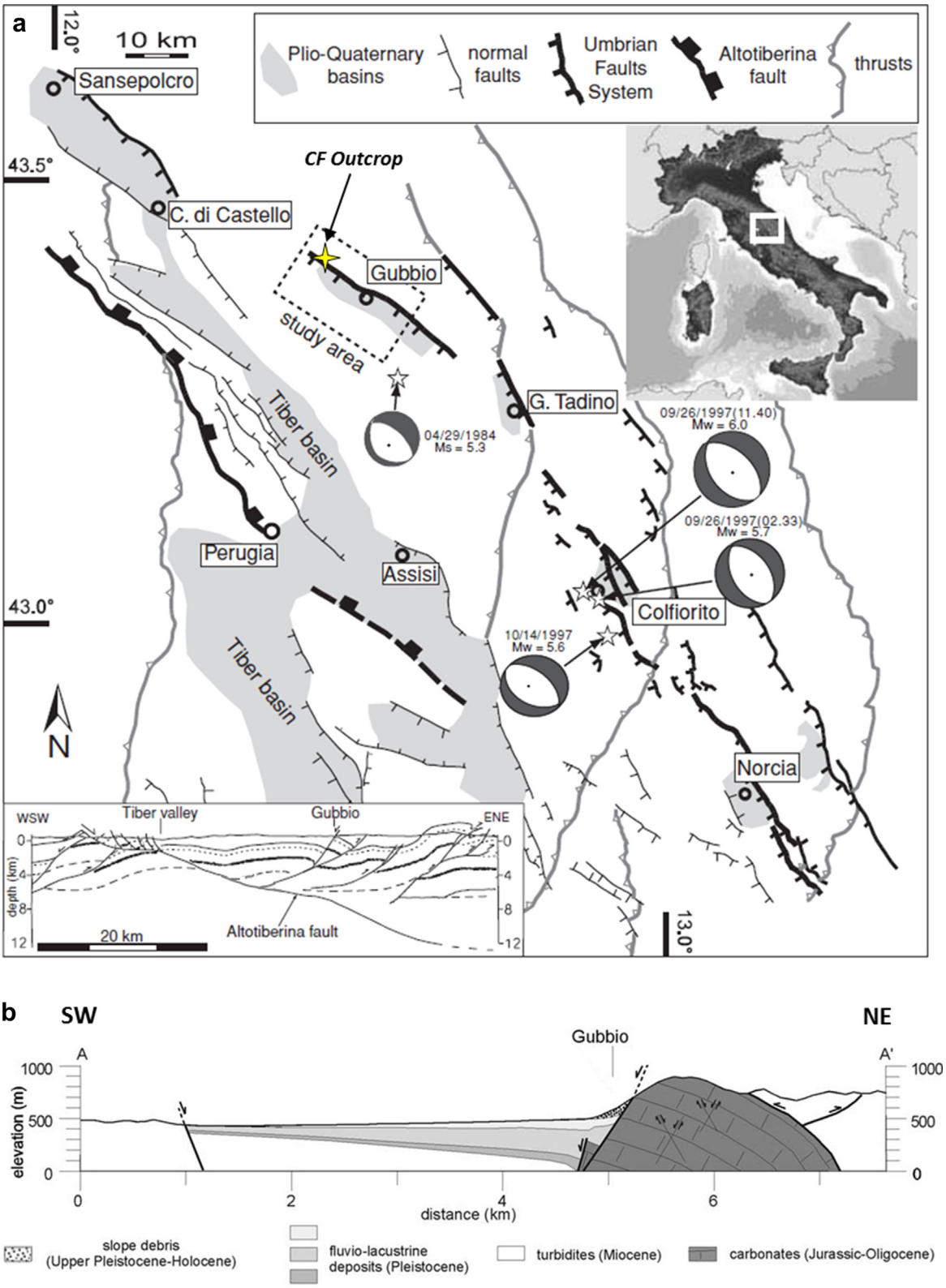

Fig. 1. a) Schematic structural map of the Umbria region (from Pucci et al., 2003, after Barchi et al., 2001), showing location of study area. Focal mechanisms and magnitudes are for the 1997 Colfiorito sequence (Ekström et al., 1998) and the 1984 Gubbio earthquake (Dziewonski et al., 1985). The location of the Cava Filippi (CF) outcrop is indicated. Inset is a schematic regional geologic section, constructed with the aid of seismic profile interpretations (modified from Boncio et al., 1998). b) Geological cross-section of the Gubbio fault, with the Gubbio Basin to the west in the hangingwall and the Gubbio anticline to the east in the footwall (modified from Collettini et al., 2003).

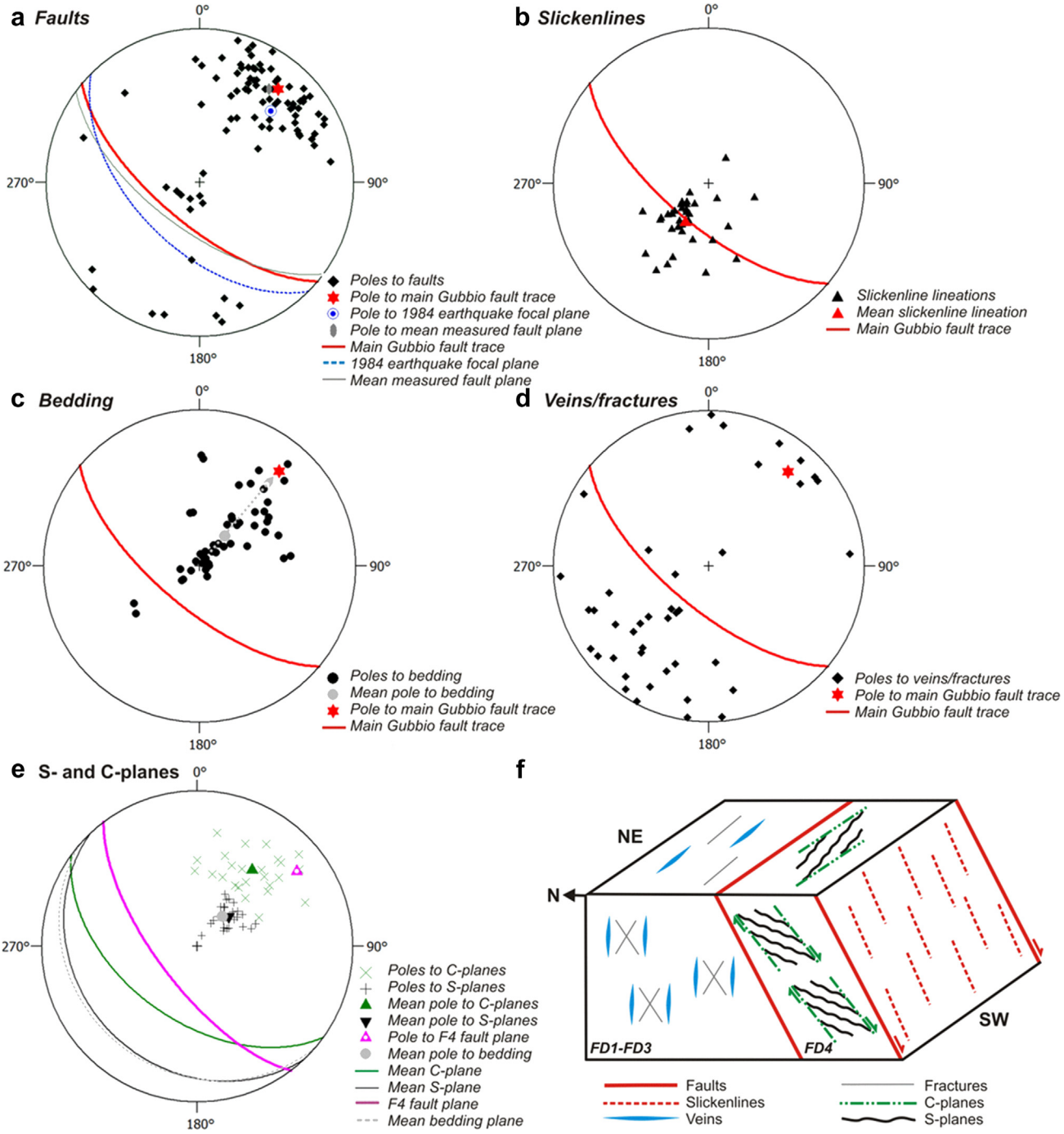

Fig. 2. a–e are equal area, lower hemisphere stereographic projections of the main structural features related to the Gubbio normal fault. Measurements are taken from both the damage zone (in the case of bedding, veins/fractures and faults) and from within the fault core. The trace of the main Gubbio fault is plotted on projections a–d as a reference. a) PSSs and subsidiary faults. The mean trend of the measured faults is consistent with the trend of the main Gubbio fault trace (Collettini et al., 2003) and the focal plane of the 1984 Gubbio earthquake (Westaway et al., 1989), which are also plotted. b) Slickenlines on fault surfaces, plunging steeply SW in a pure dip-slip geometry. c) Bedding: rotation of bedding from the protolith to the fault core is highlighted by the dashed arrow. d) Fractures and veins. e) C- and S-planes of the S–C fabric in FD4, and also observed within the slip zones of F3 and F4. The plane of F4 and the mean bedding plane are also plotted. f) Block diagram summarising the angular relationships between the structures observed at Gubbio, all of which have kinematics consistent with extension related to movement on the Gubbio normal fault.

this event was attributed to movement on the Gubbio fault (e.g. Collettini et al., 2003). A temporary seismic network installed three days after the main event recorded ~300 aftershocks ($M < 3.5$), arranged in two linear clusters trending sub-parallel to the strike of the Gubbio fault: a northern cluster (10 km long and 3 km wide in map view), where seismicity was limited to depths of 1–4 km, and a denser southern cluster (14 km long and 5 km wide), where seismicity was limited to depths of 4–6 km (Collettini et al., 2003). The aftershocks were located in the hangingwall of the Gubbio fault, rather than on the fault plane itself, and thus were interpreted to represent stress readjustments within the fault hangingwall (Pucci et al., 2003). Microseismicity has been recorded in the Gubbio area during a survey conducted from October 2000–May 2001 (Piccinini et al., 2003), which allowed

Chiaraluce et al. (2007) to clearly image the subsurface geometry of the northern portion of the Gubbio fault. The Umbria fault system has hosted two other major normal-faulting events during recent decades: the Norcia earthquake in 1979 (Mw = 5.8) (Deschamps et al., 1984), and the Colfiorito seismic sequence from 1997 to 1998 (Mw < 6.0) (Amato et al., 1998). In addition, the 2009 L'Aquila (Mw = 6.1) (Chiarabba et al., 2009) earthquake was located ~130 km SE of Gubbio on the Paganica fault, also part of the Apennine fault system. Real-time slip analyses using LiDAR-based methods showed that the latter earthquake was succeeded by slow, afterslip deformation in the months following the earthquake (Wilkinson et al., 2010; D'Agostino et al., 2012). All of these seismic events nucleated in and propagated through the Mesozoic–Cenozoic carbonatic multilayer bedrock sequence.

The outcrop that forms the focus of this present study is at Cava Filippi (43°23′21.95″N, 12°29′51.83″E), located ~1.5 km to the N of the village of Mocaiana, which lies near to the NW termination of the Gubbio fault and where the displacement on the fault is ~1.5 km (Mirabella et al., 2004). This outcrop is part of the footwall of the Gubbio fault. The fault rocks at Cava Filippi formed at depths of less than 2.5–3 km within a confined fluid system (Bussolotto et al., 2007).

3. Fault zone architecture

3.1. Terminology

Throughout this paper, certain terminologies and abbreviations are used, which we now define. Firstly, the fault core contains a number of *slip zones*, which are zones up to a few 10s of cm wide, containing variably developed brittle fault rocks (breccias, cataclasites; see below). These slip zones each contain a *principal slip zone* (PSZ), which at our study site is never greater than 1.5 mm thick. PSZs typically consist of ultracataclasite or gouge. Each PSZ is associated with a discrete *principal slip surface* (PSS), which sharply cuts the PSZ along one of its margins. The majority of displacement within the fault core is thought to be accommodated collectively along the PSSs and within the associated PSZs (e.g. Sibson, 2003; Smith et al., 2011a).

Secondly, we follow the classifications of Woodcock and Mort (2008) for brittle fault rocks that are defined primarily by grain size. A cohesive fault rock with ≥30% large clasts (≥2 mm in diameter) is classified as a breccia. Anything with <30% large clasts is a cataclasite, and different classes of cataclasite are defined according to the ratio of small clasts (0.1–2 mm in diameter) to cement/matrix (clasts < 0.1 mm in diameter). A fault gouge is defined as a fine-grained fault rock that is incohesive (Woodcock and Mort, 2008). The breccias are further subdivided based on how well the clasts fit together. In *crackle breccias*, the clasts are separated by thin seams of cement/matrix and have little evidence for rotation of clasts. In *mosaic breccias*, clasts display greater separations and rotations, but adjacent clasts can fit back to their original configuration. In *chaotic breccias*, clast separation and rotation are so large as to preclude reassembly by visual inspection. In addition to these random-fabric fault rocks, we also describe a number of foliated brittle fault rocks, where the fabrics are a result of pressure-solution processes dominating over brittle processes.

3.2. Protolith

Here we refer to the protolith as the "relatively undeformed" host rock, where brittle deformation is at a background level. The hangingwall rocks, which are not exposed in the study area, are Quaternary-age lacustrine and fluvial deposits of the Gubbio Basin, which range from clay-rich lignites through to sandstones and conglomerates (GE.MI.NA, 1963). Protolith rocks in the footwall of the Gubbio fault dip gently to the NE (Fig. 2c).

The rocks deformed within the fault core of the Gubbio fault belong to the Scaglia Rossa Formation. The Scaglia Rossa Formation is part of a Jurassic to Oligocene carbonate succession in the Umbria–Marche Apennines (Collettini et al., 2003). It consists of Turonian to Danian pale grey–red, micritic limestones with regular marl interbeds up to several cm thick (Bortolotti et al., 1970; Trabucho-Alexandre et al., 2011). The two deformed members in our study area are a "micritic limestone" member (Fig. 3a), which consists predominantly of beds (up to 20 cm thick) of micritic limestone (~5 wt.% clay; marl interbeds are infrequent), and the "marly limestone" member (Fig. 3b), which is generally more thinly bedded (beds average 5–10 cm thick) and contains frequent marl-rich horizons of up to 2 cm thick. Thus, portions of the fault core derived from the marly limestone have a more significant phyllosilicate content (up to ~20 wt.%) compared to those portions derived from the micritic limestone.

3.3. Damage zone

We refer to the damage zone as the portion of the fault zone in which the protolith has been variably fractured during fault-related deformation. Several fracture sets are present, some of which emanate from the earlier compressional phase of deformation that resulted in the formation of the Gubbio thrust and anticline (De Paola et al., 2006). Here, we describe only those features that are clearly attributed to the current extensional phase of deformation. The damage zone is ~220 m wide, corresponding to a region measured from the damage zone-fault core boundary, where fracture/vein density values peak at ~15 fractures counted per metre on a 1-D transect (Sagi, 2012), to the protolith, where fracture/vein density decays to background values (<2 fractures/m, Sagi, 2012). The fractures are predominantly pure dilational features (Sagi, 2012) and are often infilled by calcite; calcite mineralisation locally forms up to 75% of the rock volume. A few shear-extensional fractures are present with offsets up to 5 mm (Sagi, 2012), as well as some dip-slip faults with displacements of up to 5 m (Sagi, 2012). All fractures, veins and faults strike subparallel to the main Gubbio fault trace, with both synthetic and antithetic dips, often displaying an Andersonian geometry (Fig. 2d). Within 2 m of the fault core-damage zone boundary, bedding starts to become highly rotated with beds being dragged into the fault core to dip at steep angles of up to 75° to the SW (Fig. 2c).

Stylolites are also noteable features within the damage zone. Typically, they are either sub-parallel or sub-perpendicular to bedding, and thus are likely a combined product of diagenesis and the prior compressional deformation phase. The stylolites in the damage zone have a high-amplitude, sutured morphology, using the classification scheme of Logan and Semeniuk (1976), with very thin seams of insoluble residue (<100 μm thick) comprising <5% of the total rock volume.

3.4. Fault core

We refer to the fault core at Cava Filippi as the part of the fault zone where the majority of the normal displacement and associated fault rocks are concentrated (Fig. 3c and d). This outcrop was selected for its excellent exposures in an active quarry, orthogonal to the main PSSs. The damage zone-fault core boundary is marked by a PSS (F1) and thus is very sharp. The fault core has a width across-strike of ~15 m, and is bounded to the SW by a major escarpment that corresponds to the unexposed trace of the Gubbio fault. Following the practice of Bussolotto et al. (2007), we subdivide the fault core in the quarry into four structural domains

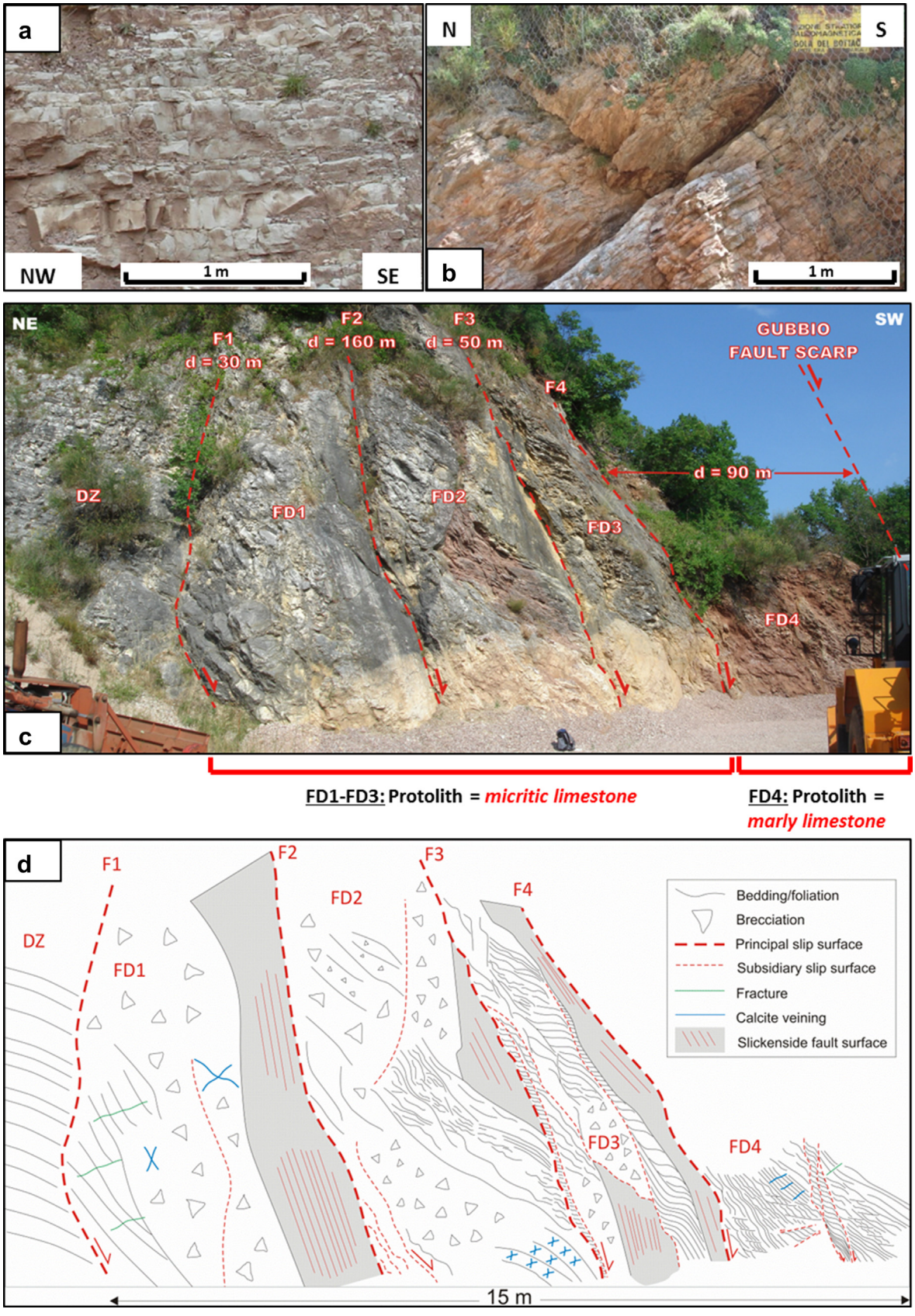

Fig. 3. a–b show photographs of the undeformed rocks of the Scaglia Rossa Formation, which represent the protolith of the rocks deformed in the fault core of the Gubbio fault: a) the micritic limestone member. b) The marly limestone member. c) Photograph of the fault core exposed at Cava Filippi, with PSSs (F1–F4) highlighted and the fault core domains (FD1–FD4) labelled. DZ = damage zone. Estimated fault/intradomain displacements, d (from Bussolotto et al., 2007), are also labelled. Colour variations in the outcrop are due to weathering and leaching rather than compositional differences. d) Schematic sketch of the outcrop shown in c, showing the main structural features. See text for description.

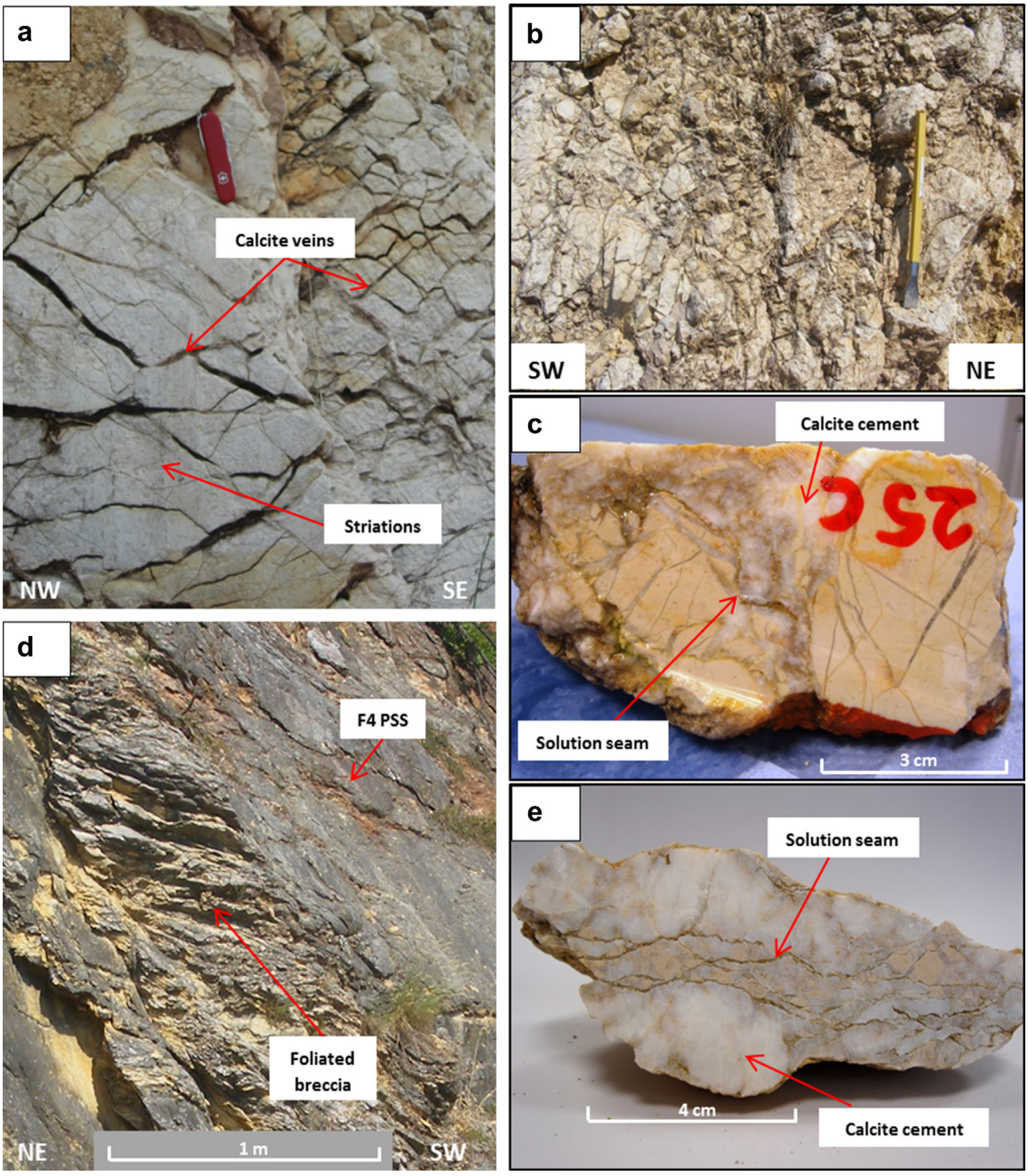

Fig. 4. Typical mesoscale features in domains FD1–FD3. a) FD1: bedding surfaces are striated. They also display several cross-cutting calcite veins, which have curviplanar geometries. b) FD2: pervasive fractures and hydrofractures created breccias and destruction of bedding. c) Mosaic breccia from FD1, although the large clast on the right-hand side displays a crackle breccia texture. Angular clasts of limestone are transected by calcite veins. A solution seam runs across the centre of the sample. d) FD3 is characterised by foliated breccias. e) Chaotic breccia from FD3 with a large proportion of calcite cement. Clay-rich solution seams define a foliation.

(FD1–FD4), delimited by four main slip zones, which are bounded by the PSSs, F1–F4 (Fig. 3c and d). FD1–FD3 are derived from the micritic limestone member of the Scaglia Rossa Formation, whereas FD4 is derived from the marly member, creating a marked lithological heterogeneity within the fault core. Bussolotto et al. (2007) used biostratigraphic controls to estimate the individual fault and intradomain displacements, which are illustrated in Fig. 3c and described in Section 3.4.1. These estimates suggest that each PSS has several tens of metres of displacement, whereas the displacement within the domains (i.e. within FD1, FD2 and FD3) between the faults is negligible. The exception is domain FD4, which, along with F4, is estimated to have accommodated up to 90 m of displacement. In total, the cumulative displacement at the Cava Filippi outcrop is estimated to be 150–230 m, which equates to ~12% of the total estimated throw of the Gubbio fault (Bussolotto et al., 2007), the remainder of the throw being accommodated by the adjacent main Gubbio fault scarp.

3.4.1. Mesostructural observations

3.4.1.1. Domains FD1–FD3 (micritic limestone protolith). FD1 is characterised by highly rotated bedding planes, which are dipping very steeply compared to the shallowly dipping beds in the adjacent damage zone, at angles of up to 75° towards the SW (Figs. 2c and 3d). Some bedding surfaces are striated, in an

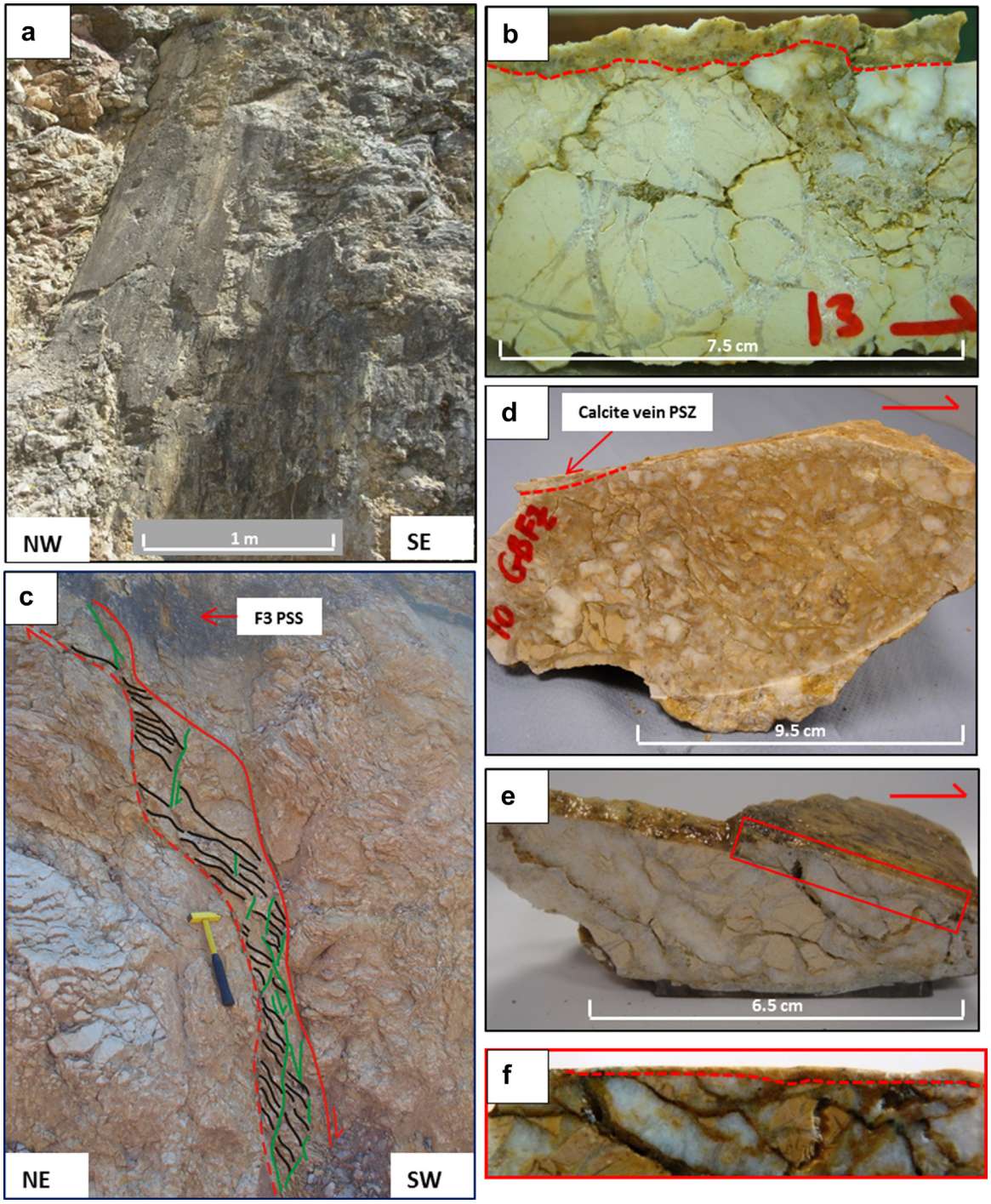

Fig. 5. Mesoscale features associated with the PSSs F1–F4. a) Fault surface of F2. b) A zone of chaotic breccia, up to 1 cm thick, underlies the PSS of F2 (PSS lies at top of sample). A layer of gouge also lay on top of the PSS but was lost during cutting. The remainder of the rock comprises a mosaic breccia. c) The slip zone of F3, which is up to 35 cm wide and displays a foliated S–C fabric (C-planes are shown in green, S-planes in black). d) A chaotic breccia from the slip zone of F3. A PSS lies along the top of the sample, and just beneath is a calcite vein-dominated PSZ, up to 5 mm wide. Clay-rich pressure-solution seams are formed at angles of up to 50° from the dip direction of the PSS and create a foliated fabric. e) Chaotic breccia and PSZ from F4. Boxed area is shown in f, to show the location of the PSZ. The PSZ is up to 1.5 mm wide and consists of ultracataclasite. Note that the pressure-solution seams displayed in d and e have a smoother morphology, and smaller amplitude to wavelength ratios, than observed in domains FD1–FD2 (see Fig. 4).

orientation consistent with slickenlines observed on the PSSs (Fig. 4a), suggesting that they have been locally reactivated as shear planes. Moving towards F2, the limestones are increasingly fractured so that bedding is almost completely destroyed leading to the development of breccias (Fig. 3d). A few relict bedding features remain in FD2. FD2 is characterised by intense fracture and hydrofracture abundance, resulting in heavy brecciation of the rocks (Fig. 4b). The exception is a patch of red, marl-rich material, with dimensions of $\sim 1 \times 2.5$ m (Fig. 3c), which displays characteristics similar to those described for FD4 (Section 3.4.1.3).

We measured fracture densities across the fault core along a 1-D transect. Fracture density in domains FD1–FD2 is ~51 fractures/m, three times greater than observed in the flanking damage zone. Fractures and veins throughout FD1–FD2 are present in two

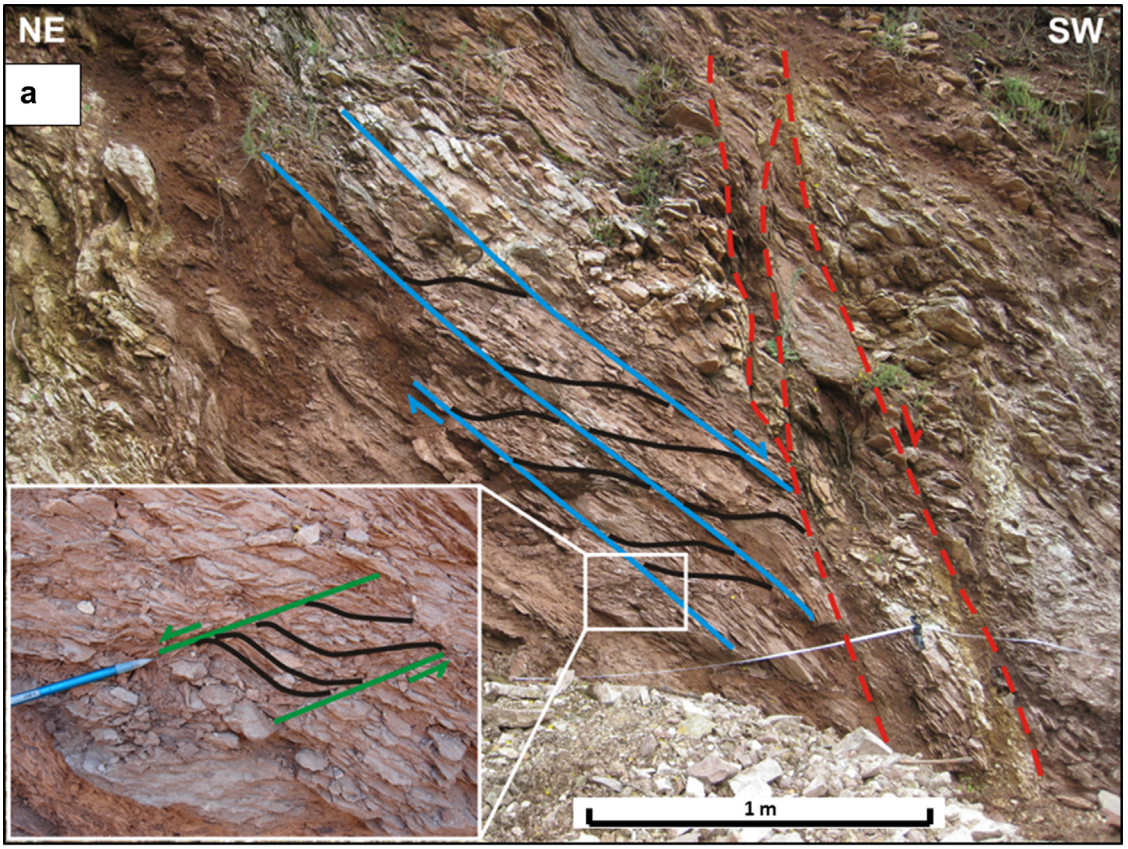
NE
SW
a
1 m

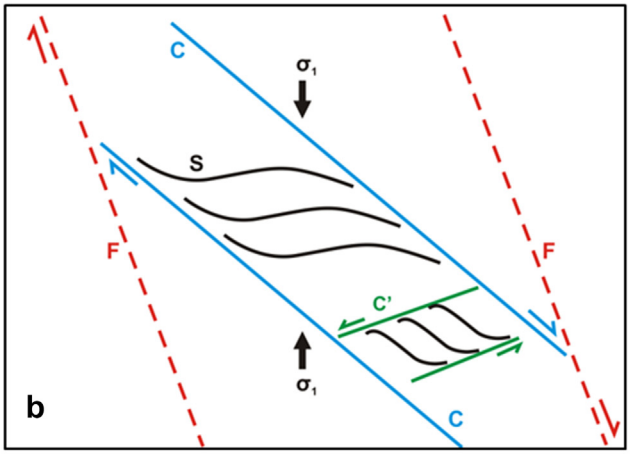
C
σ1
S
F
F
C'
σ1
C
b

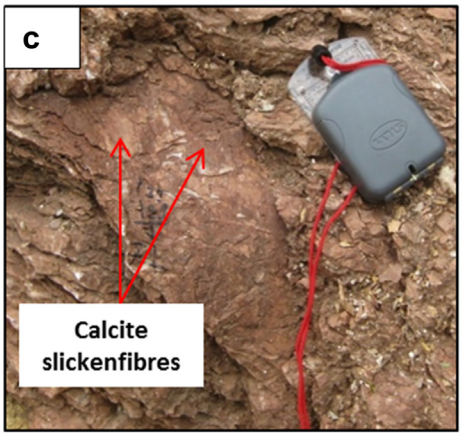
c
Calcite
slickenfibres

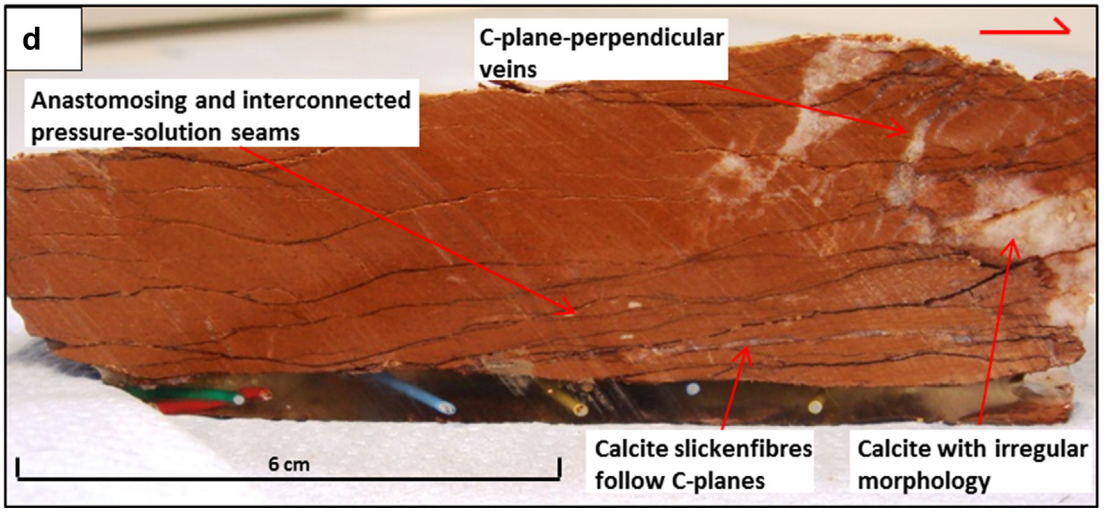
d
C-plane-perpendicular
veins
Anastomosing and interconnected
pressure-solution seams
6 cm
Calcite slickenfibres
follow C-planes
Calcite with irregular
morphology

dominant sets, as in the damage zone. Both strike NW–SE (sub-parallel to the principal slip surfaces), with one set dipping SW whereas the other dips antithetically to the NE (Fig. 2d and f). The veins have a curviplanar geometry, are up to 2 cm wide, and are filled with calcite (Fig. 4a). Several subsidiary slip surfaces occur in FD2 (Fig. 3d), and constraining the displacements for each was not possible, but the lack of any well-developed slip zones and associated gouges or cataclasites suggests that displacements are small, probably less than a few mm.

The breccias in FD1–FD2 range in composition from 30 to 70% limestone clasts, set in a crystalline calcite cement, and range from mosaic to chaotic breccia types (Fig. 4c). Limestone clasts are very angular and randomly oriented, ranging from <1 mm up to 10 cm in diameter. Clasts are commonly transected by several very fine calcite veins, which are typically <1 mm thick. This geometry creates a crackle breccia texture in certain clasts within the host mosaic/chaotic breccias (Fig. 4c). Individual crystals within the calcite cement may be visible with the naked eye and are up to 5 mm in diameter. At the mesoscale, it is difficult to differentiate between what may be clasts of calcite and the calcite cement. Intermittent clay-rich pressure-solution seams are also present, constituting ~5% of the rock volume (Fig. 4c). Where bedding features are still present, the solution seams are sub-parallel and sub-perpendicular to the bedding, consistent with the geometries observed in the protolith. However, where bedding surfaces have been reactivated as shear planes, solution seams are at angles of ~40° to the plane.

Domain FD3 is characterised by coarsely foliated breccias (Fig. 4d). They range from mosaic- to chaotic-type and the foliation is defined by anastomosing pressure-solution seams (Fig. 4e), which dip at angles ranging from ~20 to 40° to the SW, thus creating an angle of 30–50° to the dip of the PSSs (Fig. 4d). Calcite mineralisation in veins and breccia cements represents 25–85% of the rock volume and limestone clasts range from 10 to 65%. Again, clasts are angular and display a wide range of sizes from <1 mm up to 5 cm. The solution seams have a spacing of ~5 cm and locally comprise up to 10% of the bulk rock volume. Solution seams within FD1–FD3 (Fig. 4c and e) typically have lower amplitude to wavelength ratio compared to those in the damage zone, and hence have a smoother, less sutured morphology. They are also noticeably thicker, being up to 3 mm wide, and occasionally contain visible fragments of calcite and limestone (<1 mm in size). Fracture density in FD3 is ~0.3 fractures/m, slightly lower than in domains FD1–FD2.

3.4.1.2. Slip zones and PSSs, F1–F4 (micritic limestone protolith). F1–F4 are discrete shear planes, and >10 m in length based on available exposure, which cut sharply through the outcrop (Fig. 5a). F1 (displacement = 3 ± 27 m, Bussolotto et al., 2007) lacks a well-developed slip zone, but a PSZ is present, consisting of a clay-rich gouge, up to 2 mm thick and containing sub-mm clasts (~25%) of calcite and limestone, coats the slip surface. F2 (displacement = 130 ± 30 m, Bussolotto et al., 2007) also lacks a well-defined slip zone, although in hand specimen, a zone up to 1 cm thick of chaotic breccia is observed immediately underlying the PSS (Fig. 5b). This brecciated zone comprises clasts of chert (20%), limestone (15%) and calcite (10%), averaging 1 mm in size, set in a calcite cement (55%). Again, the PSZ consists of a clay-rich gouge layer up to a few mm thick, which coats the PSS.

F3 (displacement ≤ 50 m, Bussolotto et al., 2007) has a slip zone up to 35 cm wide, which has a foliated S–C fabric (Fig. 5c). The C-planes are defined by shear planes running sub-parallel to F3, and the S-planes are defined by phyllosilicate-rich pressure-solution seams that constitute up to 10% of the rock volume. They form at angles of up to 50° from the dip of F3 and have average spacings of ~1.5 cm (Fig. 5d). Within the lithons bounded by the foliation, the rock is composed of angular clasts of limestone (15%) and calcite (30%) formed from fragmented calcite veins and/or cement, typically <5 mm in size, set in a calcite cement (55%). Given that 30% of the clasts are fragmented veins or cement, then this rock can be classified as a chaotic breccia. F3 has a PSZ up to 1 mm wide, defined by a layer of calcite veining (up to 0.5 mm wide) (Fig. 5d), plus a ~0.5 mm thick gouge layer.

F4 (displacement of 60 ± 30 m along with FD4) also has a slip zone up to 50 cm wide, associated with an S–C foliated chaotic breccia (Fig. 5e). Here, angular limestone and calcite clasts comprise up to 30% each and the calcite cement comprises ~40% by volume. Clasts range from <1 mm to 3.5 cm diameter, averaging ~5 mm in size. Some clasts can still be fitted back together in a jigsaw geometry. The phyllosilicate-rich pressure-solution seams are oriented at angles of up to 30° from the dip of F4 (Fig. 5e), and are often very closely spaced (average spacing ~5 mm). This high density means that the clay seams locally form up to 15% of the rock volume. In addition, the least-weathered parts of the fault exhibit a PSZ up to 1.5 mm wide composed of ultracataclasite (Fig. 5f). The PSSs of F1–F4 are often heavily mineralised, displaying calcite slickenfibres in addition to slickenlines that both indicate predominantly dip-slip fault movement (Figs. 3b and 5a).

3.4.1.3. Domain FD4 (marly protolith). In FD4, which is derived from the marly limestone, the deformation style is very different. Compared to other parts of the fault core, fractures are not abundant and shear localisation along through-going faults is rare. Instead, the deformation is represented by a continuous and pervasive S–C fabric (Fig. 6a). The C-planes have an average strike direction that is sub-parallel to the domain-bounding PSSs (Figs. 2e, f, 6a and b), but they dip at a shallower angle, which is explained by the fact that they appear to have reactivated the pre-existing bedding planes that rotated during deformation. The C-planes are defined by an anastomosing network of clay-rich pressure-solution seams (Fig. 6d). Individual seams are up to a few mm thick. Many C-planes have calcite slickenfibres precipitated on their surfaces (Fig. 6c), which display kinematics consistent with that of the main fault zone, i.e. dip-slip extensional. The S-planes are also defined by seams of pressure-solution, which are generally <1 mm thick (Fig. 6d). They are inferred to have formed perpendicular to the direction of the local maximum principal stress induced by shearing along the C-planes (Fig. 6b). A less well-defined C′-type shear band cleavage locally overprints the primary S–C fabric (Fig. 6a and b). The spacing of the C-foliation ranges from <1 mm up to 2 cm, so that in some places, the clay-rich seams comprise up to 20% of the rock volume. In contrast to the pressure-solution seams in domains FD1–FD3 and in the damage zone, the seams in FD4 have a very smooth, anastomosing morphology (Fig. 6d).

Fig. 6. Mesoscale features associated with domain FD4. a) Deformation is distributed throughout the domain via a continuous, foliated S–C fabric. Inset shows the detail of a local and less well-defined C′-type shear band cleavage. A localised shear zone cuts through the domain on the right-hand side of the image (red-dashed lines). b) Kinematic summary of the main structures observed in FD4. c) Calcite slickenfibres precipitated on the surface of a C-plane provide evidence for fluid-assisted shearing along the plane. d) Hand sample from FD4, showing the internal structures within a lithon bounded by two S-planes. C-planes, defined by phyllosilicate-rich pressure-solution seams anastomose through the rock, creating interconnected networks. Calcite mineralisation is present, but less so than observed in domains FD1–FD3. Veins are typically perpendicular to the C-planes and have a tabular morphology, but occasional patches of calcite with an irregular morphology are present. Calcite slickenfibres are again present along C-planes. (For interpretation of the references to colour in this figure legend, the reader is referred to the web version of this article.)

This geometry is consistent with the relatively phyllosilicate-rich nature of the marls in FD4, since higher clay content promotes the pressure-solution process (e.g. Rutter, 1976) and favours the development of non-sutured morphologies (Logan and Semeniuk, 1976).

Calcite mineralisation is present but much more sparse than in FD1–FD3. Calcite veins only constitute up to 20% of the rock volume and they tend to be much narrower than those in FD1–FD3, typically <5 mm wide. They are formed predominantly perpendicular to the C-planes (Figs. 6d and 10a). The veins generally have a tabular morphology, although irregular forms are also present (e.g. Fig. 6d). The exception to the predominantly distributed deformation is a localised shear zone that cuts through the centre of FD4 (Fig. 6a). This shear zone, ~25 cm wide, is bounded by two slip surfaces. However, the foliated nature of the rocks within this shear zone does not differ significantly to those seen throughout FD4.

3.4.2. Microstructural observations

3.4.2.1. Domains FD1–FD3 (micritic limestone protolith). Optical microscope analysis shows that the limestone clasts in the breccias have reduced sizes of <100 μm and are always very angular shapes. They are extensively fractured and transected by fine calcite veins ranging from 10 μm up to a few mm wide (e.g. Fig. 7a). Consistent with the observations made at outcrop scale, these veins form conjugate sets. The calcite veins typically have a blocky texture, and occasionally an elongate blocky texture (Fig. 7a). The size of the crystals depends on the width of the vein, but they may be up to 500 μm in diameter in the centre of the widest veins, generally with smaller crystals at the vein boundaries (Fig. 7a). Veins typically have a discontinuous and/or branching geometry (Fig. 7a).

The nature of the calcite crystals within the breccia cement contrasts significantly compared to the vein crystals. Calcite crystals in the cement are mostly anhedral with random orientations (Fig. 7b). They are also highly inequant, ranging from <20 μm up to 5 mm in size. In addition, deformation twins are common within the calcite cement, particularly in the largest crystals, and they may be >1 μm thick and can be curved and taper out within crystals (Fig. 7b). Although several twins correspond to type I deformation twins of Burkhard's (1993) classification, which is consistent with deformation at temperatures < 200 °C, ~50% correspond to type II–type III deformation twins. Typically type II–type III deformation twins are associated with temperatures of deformation in the range 150–250 °C, which is high considering the 2.5–3 km of exhumation for the Gubbio fault. Further, Bussolotto et al. (2007), used palaeothermometric techniques to calculate temperatures of formation of the fault rocks at Cava Filippi of <50 °C. Thus, we infer that the high-strain rates experienced within the fault core enhanced deformation twin morphology (e.g. Rybacki et al., 2013).

Pressure-solution seams average 50 μm to 1 mm wide and are filled with an extremely fine-grained crystal aggregate. EDX analysis with the SEM shows that the seams comprise up to 80% phyllosilicate with the remainder being very fine-grained calcite crystals. Calcite crystals are quite equant, ranging from ~25 to 50 μm in diameter, and are sub-rounded (Fig. 7c). Bearded overgrowths (Fig. 7d) occur in some solution seams in domain FD3, suggesting that pressure-solution creep is likely an active deformation mechanism within this domain. The solution seams typically cross-cut all other structures (i.e., clasts, cement, veins) in the breccias, indicating that they continued to develop after most other structures.

3.4.2.2. PSZs, F1–F4 (micritic limestone protolith). PSSs appear as very sharp, straight boundaries that truncate all features within the host breccias (Fig. 8a). As described in Section 3.1, the PSS bounds a PSZ. The PSZs observed in this study range from ~0.5 to 1.5 mm thick and are one of two types: those defined by zones of ultracataclasite and those defined by PSS-parallel calcite veins.

F4 is an example of an ultracataclasite-dominated PSZ (Fig. 8a) with four well-defined sub-zones. Sub-zone 1, which ranges from 515 to 915 μm wide, consists of ultracataclasite. The ultracataclasite has a random fabric and contains sub-rounded clasts of limestone (10%) and calcite (50%) set in a matrix (40%) of ultrafine-grained calcite and clay (Fig. 8c). Clasts range from 20 to 600 μm in size. Anything less than 20 μm in size is attributed to the matrix. Sub-zones 2, 3 and 4, which have widths of up to 430 μm, 240 μm and 220 μm, respectively, consist of discontinuous, blocky calcite veins that contain crystals ranging from ~40 to 800 μm in size. Each sub-zone is bounded by a slip surface. These surfaces are highlighted by the presence of an orange–brown material (Fig. 8d), which at high magnification, and with the SEM, is seen to consist of sub-rounded calcite crystals, <20 μm in size, dispersed within phyllosilicate-rich material. The calcite crystals within this material do not appear to have been particularly fractured or abraded, and many of them have concave boundaries.

SEM investigation of the uppermost slip surface corresponding to the striated F4 plane observed in the field reveals a more complex structure. It shows the presence of an ultrafine-grained, phyllosilicate-rich gouge lining the slip surface (Fig. 9a), and this gouge displays further sub-zones, which we refer to here as "shear localisation zones" (SLZs) 1 and 2. SLZ 1, which is up to 15 μm thick, has a phyllosilicate content of ~50%, in which the phyllosilicates are randomly oriented, and contains sub-angular calcite clasts up to 20 μm in diameter. SLZ 2, which is <5 μm thick, is much finer-grained, containing nano-sized clasts of calcite, which have a smooth and asymmetric shape (Fig. 9a). These clasts are surrounded by finely foliated phyllosilicates, which comprise ~80% of SLZ 2. Also within SLZ 2, several shear surfaces are preserved (Fig. 9a). In some specimens from F4, we observed sub-spherical pores within the SLZs that resemble bubbles, which are surrounded by elongate calcite crystals and a small amount (<20%) of phyllosilicate (Fig. 9c). Other parts of the SLZs preserve "dog-bone" or "H"-shaped calcite crystals (Fig. 9d). SEM analyses have also been performed parallel to the slip surface of F4, i.e. looking down onto the striated fault surface. Here, we observed tightly-packed calcite grains with dimensions ranging from 50 to 150 nm, which sometimes exhibit polygonal boundaries and triple-junction contacts (Fig. 9e and f).

F3 exhibits an example of a calcite vein-dominated PSZ (Fig. 8b). The PSZ contains a number of calcite veins, which are characterised by transitions along their length over distances of <300 μm from a blocky to a fibrous texture (Fig. 8b and d). The areas of blocky calcite are characterised by crystals with an average size of 100 μm that display a crack-seal texture where fluid inclusions are aligned sub-perpendicular to the slip direction (Fig. 8d). The fibrous veins are characterised by much smaller, euhedral crystals, on average ~15 μm in size with the fibrous texture being created by micron-scale stylolitic surfaces lying sub-parallel to the PSS (Fig. 8e). Similar to F4, the slip surfaces that bound the veins within the PSZ are highlighted by the presence of orange–brown phyllosilicate and have a jagged, stylolitic morphology (Fig. 8d).

3.4.2.3. Domain FD4 (marly protolith). The pressure-solution origin of both the C- and S-planes is evident under the microscope, due to the truncation of micro-fossils (Fig. 10b). The pressure-solution seams that define the C-planes have an anastomosing morphology, creating interconnected, phyllosilicate-rich networks (Fig. 10b). Solution seam spacings range from μm to cm scale (Fig. 10a and b), thus they are much more pervasive than initial field observations suggested, as are the S-planes. The C-planes link up with the

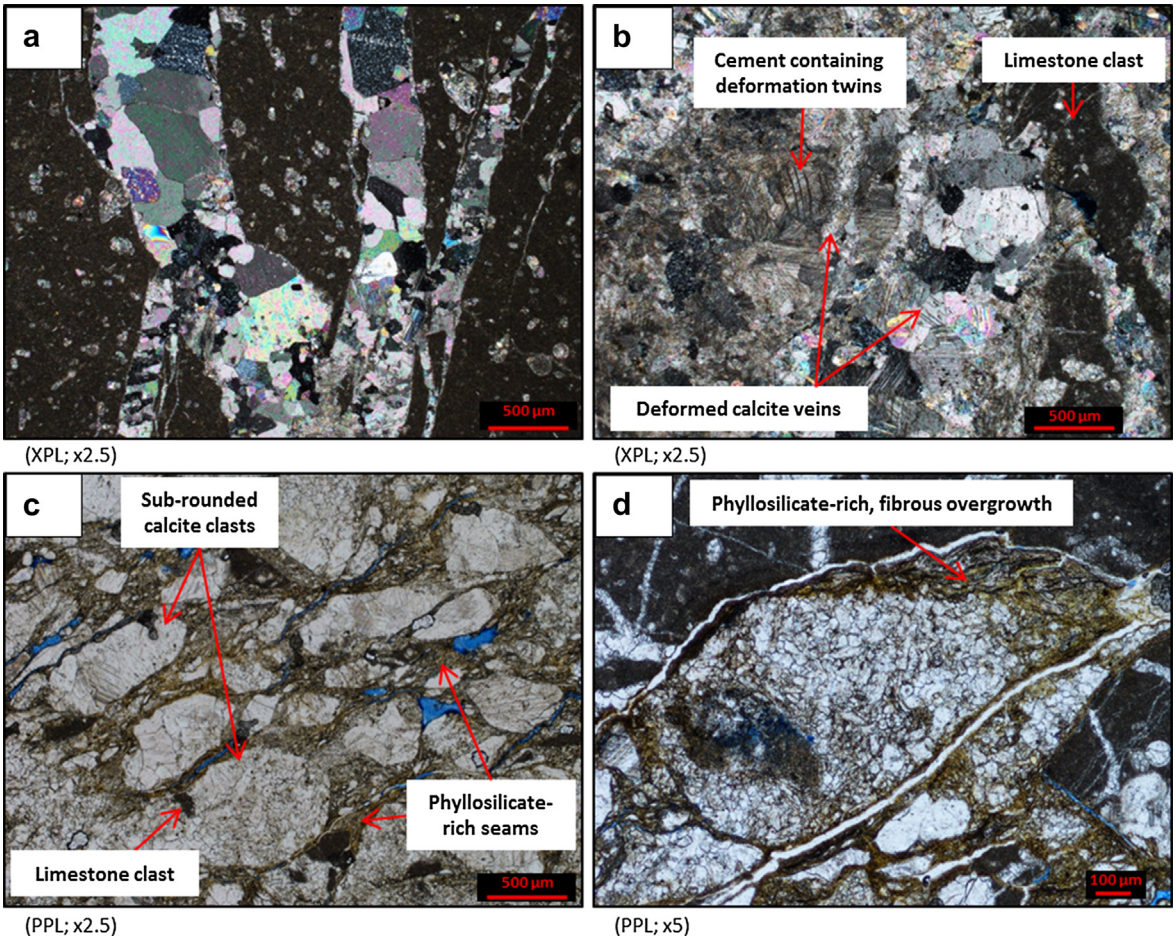

Fig. 7. Typical microscale features in domains FD1–FD3. a) Branching calcite veins, transecting a clast of limestone. They predominantly have a blocky texture, although the bottom left-hand side vein has an elongate blocky texture. Smaller crystals are often concentrated at the limestone-vein boundaries. b) Calcite cement in breccia from FD2. Calcite crystals in the cement appear much more deformed than those in the veins, typically displaying type II/type III deformation twins (Burkhard, 1993). Earlier veins were incorporated into the cement through fracturing and brecciation. c) Anastomosing phyllosilicate-rich solution seams in FD3. The dissolution of clasts of limestone and calcite produced sub-rounded shapes, compared to the typical angular clasts observed in many breccias in FD1–FD2. d) Bearded overgrowth on a clast of calcite within a pressure-solution seam from FD3.

S-planes, thus bounding lithons of relatively undeformed limestone. The solution seams that define the S- and C-planes may be up to 100 μm thick. EDX analysis shows that they are filled with ~50% phyllosilicate and 40% calcite with the remaining 10% comprising quartz and diagenetic apatite (Fig. 10d). This material is moderately foliated due to the alignment of phyllosilicate grains (Fig. 10c and d). The clasts within the solution seams have relatively smooth, concave boundaries, typical of dissolution (Fig. 10c), and show little evidence of internal deformation that contrasts with the clasts in the phyllosilicate-rich SLZs of F1–F4, which are highly fractured and have sharp, angular boundaries (Fig. 9b).

Microstructures within the solution seams are inferred to indicate two coeval deformation mechanisms. Firstly, asymmetric delamination features and micro-folds (Fig. 10c) imply foliation-parallel sliding along (001) clay lamellae. And secondly, pressure shadows around clasts (Fig. 10d) indicate the operation of pressure-solution creep. In all cases, the sense of shear interpreted from the asymmetry of these microstructures is consistent with that of the fault zone.

Calcite veins display similar characteristics to those in FD1–FD3. They have a drusy and blocky texture, ranging from <10 μm up to a few mm wide (Fig. 10a). Their consistent orientation orthogonal to the prevailing C-plane foliation is characteristic of deformation by pressure-solution. The veins are also offset by the pressure-solution seams by distances of up to a few cm (Fig. 10a). This geometry may be due to dissolution, or alternatively, some of the larger offsets may be caused by frictional sliding or creep along the solution seams.

4. Mineralogical observations

XRD analyses were performed on the clay fraction present within various parts of the fault zone to constrain what clays are present and to assess what influence clay mineral content may have on the behaviour of the different fault core domains. A total of six samples were analysed: two samples representing the protolith (one from the micritic limestone protolith and one from the marly protolith), two samples representing pressure-solution seams (one from domain FD3 and one from domain FD4), and two samples representing PSZs (one from F3 and one from F4). Sample details and results are summarised in Table 1 and representative XRD traces are shown in Fig. 11.

In the protolith, the clays present are illite, mixed-layered illite-smectite and a very small amount (<1%) of kaolinite. These same clays are present in the pressure-solution seams from both domains FD3 and FD4, although the solution seams show a relative enrichment of kaolinite (up to 25%). However, a significant difference in clay content is observed within the PSZs of F3 and F4. Whilst illite and kaolinite are still present, smectite forms only 2%

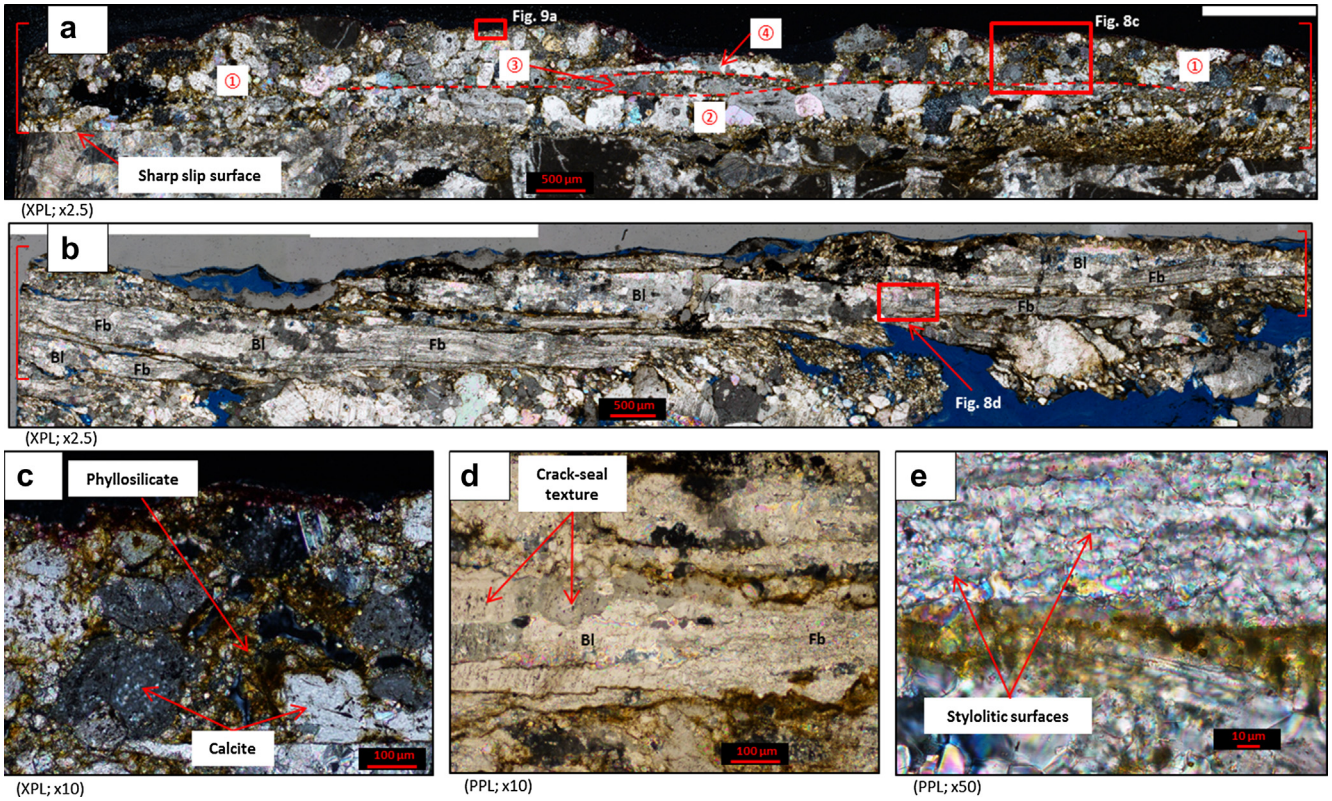

Fig. 8. Typical microscale features associated with the PSSs F1–F4. a) Example of an ultracataclasite-dominated PSZ (bracketed) from F4 (hand sample is shown in Fig. 5e and f). Note the very sharp boundary between the host breccia and the PSZ on the left-hand side of the image. This becomes less sharp towards the right-hand side as the slip surface is overprinted by pressure-solution. This PSZ comprises four sub-zones, labelled 1–4, which are bounded by discontinuous slip surfaces, highlighted in red. Sub-zone 1 is dominant and consists of ultracataclasite (see fig. c). Sub-zones 2–4 are discontinuous and consist of blocky calcite veins. b) Example of a calcite vein-dominated PSZ (bracketed) from F3. A number of calcite veins are present. Veins are characterised by transitions (see fig. d) from a blocky texture to a fibrous texture along their length (labelled Bl = blocky; Fb = fibrous). The blocky calcite veins contain crystals averaging 100 µm in diameter, displaying a crack-seal texture (see fig. d). The fibrous calcite veins contain much smaller, euhedral crystals, averaging 15 µm in diameter (see fig. e). c) Close-up image of the ultracataclasite in the PSZ of F4 (location shown in a). It contains sub-rounded clasts of calcite in a matrix of ultrafine-grained calcite and clay. d) Close-up image of transition between blocky (Bl) and fibrous (Fb) calcite (location shown in b). The alignment of fluid inclusions that creates the crack-seal texture in the blocky calcite can be seen. The orange–brown material is interpreted to be a product of pressure-solution along planes sub-parallel to the PSS/vein boundaries. e) Close up of fibrous vein, showing the jagged stylolitic surfaces that create the fibrous texture. Again, the orange–brown material is inferred to be from pressure-solution between slip surfaces. (For interpretation of the references to colour in this figure legend, the reader is referred to the web version of this article.)

of the clay fraction within the PSZ of F4 and is completely absent within the PSZ of F3. These results are consistent with the chemical compositions obtained by in-situ EDX analyses of the clay minerals.

5. Discussion

5.1. Deformation styles and mechanisms

Three dominant styles of deformation are recognised within the core of the Gubbio fault. Domains FD1–FD3, derived from the micritic protolith, are characterised by pervasive fractures, veins and chaotic breccias. Other features include intermittent pressure-solution seams and subsidiary slip surfaces. The style of deformation is thus *discontinuous* and *distributed*. The main deformation mechanisms inferred from microstructural observations are fracturing and hydrofracturing, with minor amounts of diffusive mass transfer and local frictional sliding along minor faults.

The slip zones of F1–F4, also derived from the micritic limestone protolith, are up to 50 cm wide, containing chaotic breccias, which can also have a coarsely foliated S–C fabric. They each contain a PSS and an associated PSZ. PSZs are up to 1.5 mm wide, containing variable amounts of ultracataclasite and gouge, together with slip surface-parallel calcite veins. Even narrower SLZs (<5 µm wide) are observed within the PSZs. Thus, the deformation is *discontinuous* and *localised,* with the main inferred deformation mechanisms being cataclasis and frictional sliding. The foliated S–C fabrics within the slip zones and the development of phyllosilicate-rich stylolitic surfaces along some PSSs (e.g. that of F3 described in Section 3.4.2.2) indicate that diffusive mass transfer processes also play a role within the slip zones F1–F4.

In domain FD4, derived from the marly protolith, the style of deformation is very different to that observed in the rest of the fault core. The main deformation product is a pervasive S–C foliation, where the foliation is defined by abundant pressure-solution seams. The style of deformation is thus *continuous* and *distributed*, with the inferred dominant deformation mechanism being pressure-solution.

5.2. Lithological controls on deformation mechanisms and frictional behaviour

Our findings illustrate that marked contrasts in both the deformation styles and dominant deformation mechanisms occur across the fault core, and we correlate these contrasts to changes in lithology across the core. Also, the displacement distribution estimated by Bussolotto et al. (2007) appears to be influenced by lithology because for FD1–FD3 dominated by the micritic limestones, displacement is focused on domain boundaries (i.e. along the PSSs F1–F4), whereas for FD4, significant displacement is

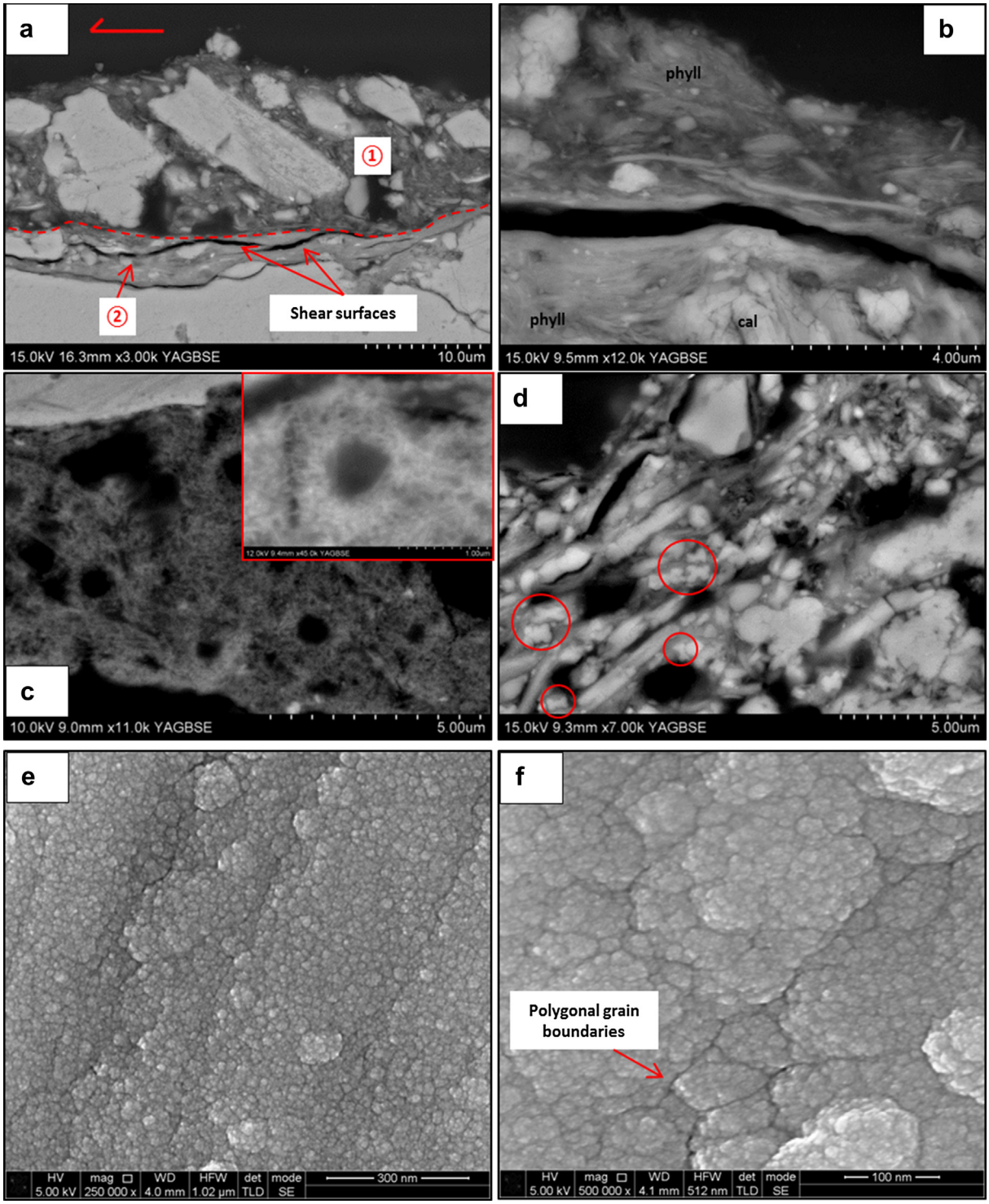

Fig. 9. SEM images of features found along the PSSs F1–F4. a) The gouge that lines the PSS of F4 (see Fig. 8a for location) comprises two SLZs that are numbered in the photograph. b) A close-up image of a SLZ, showing the fractured nature of the calcite clasts and the foliated nature of the phyllosilicates. c) Another SLZ within the PSZ of F4 contains sub-spherical pores, surrounded by a combination of elongate calcite crystals and phyllosilicate. Inset shows a close-up image of one of these pores. d) "Dog-bone"/"H"-shaped calcite crystals (highlighted by red circles). e) Image taken parallel to the PSS of F4 showing striations on the slip surface from the top right-hand side to the bottom left-hand side of the image. The grooves and ridges between striations are composed of nanoparticles of calcite. f) Close-up image of the nanoparticles that form the slip surface in e. The particles, which have dimensions ranging from 50 to 150 nm, are tightly packed with sub-polygonal boundaries and triple-junction contacts. The smaller 10–20 nm grains are an artefact of the coating applied to the sample prior to analysis. (For interpretation of the references to colour in this figure legend, the reader is referred to the web version of this article.)

accommodated within the domain. Thus, with respect to the behaviour of the Gubbio fault during the seismic cycle, we now focus our discussion on those parts of the fault core where most of the displacements appear to be concentrated, i.e. F1–F4 and FD4. Although the total displacement accrued at the Cava Filippi outcrop only amounts to ~12% of the total displacement of the Gubbio fault, the structures here are considered analogues for what may be encountered either along-strike or down-dip of the main Gubbio

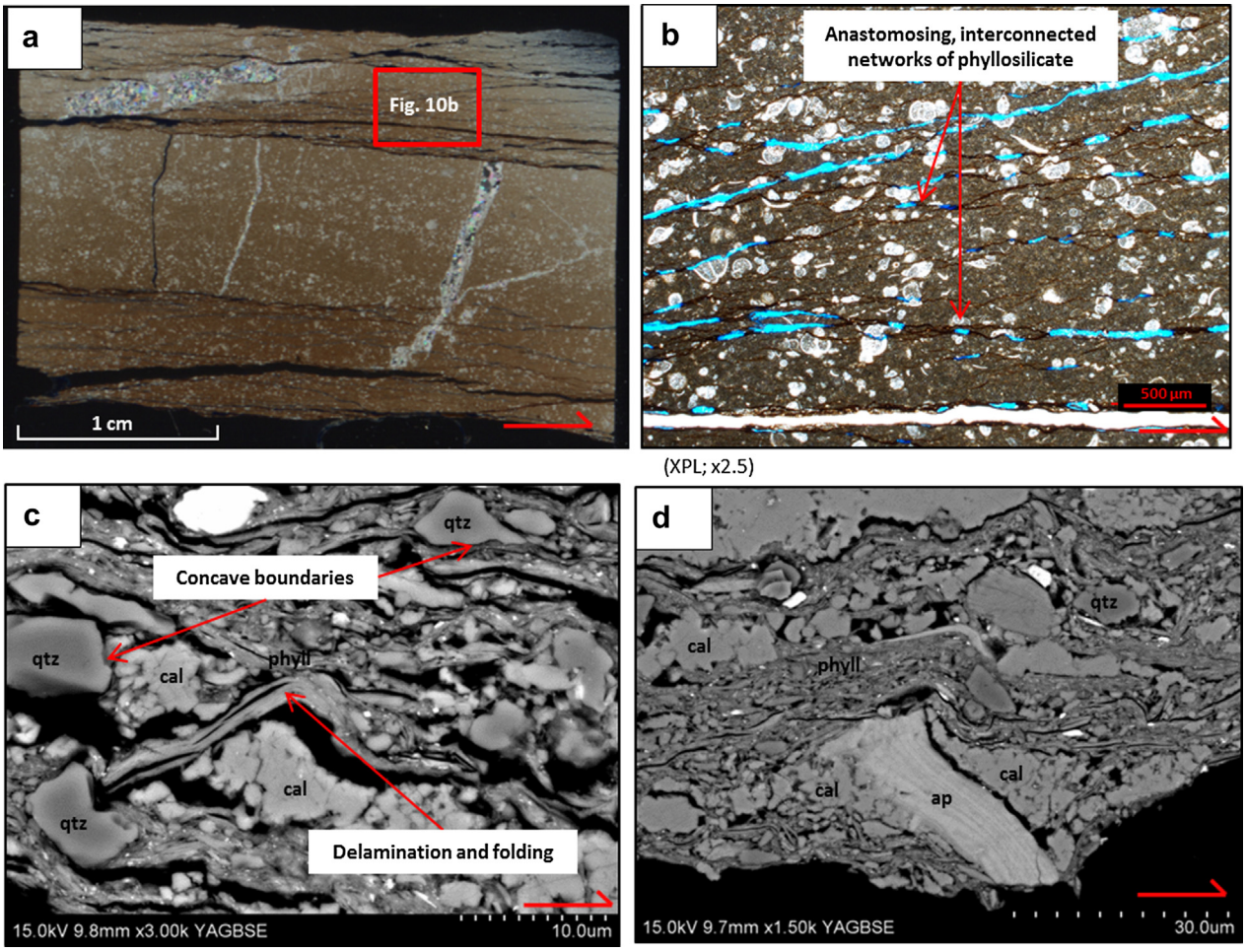

Fig. 10. Typical microscale features in domain FD4. a) Thin section scan (crossed polars) of foliated marly limestone from within a lithon bounded by S-planes. Calcite veins trend predominantly sub-perpendicular to the C-planes and are offset by up to a few mm due to pressure-solution along the C-planes. b) Optical microscope image of the foliated marly limestone (see fig. a for location). Truncation of fossils is observed adjacent to solution seams. The pressure-solution seams anastomose, bounding lithons of relatively undeformed limestone. c) SEM image of typical microstructures within the pressure-solution seams. Phyllosilicates exhibit delamination and folds/kinks, and quartz grains display smooth concave boundaries. d) SEM image showing a pressure shadow around a grain of apatite within a pressure-solution seam. The shadows on either side are composed of calcite. The alignment of phyllosilicates within the seams is the foliation. (ap = apatite; cal = calcite; phyll = phyllosilicate; qtz = quartz).

fault scarp as it traverses lithological heterogeneities in the host rock. To better understand the possible behaviour of the Gubbio fault during the seismic cycle, we compare our field, microstructural and mineralogical observations with previous studies of active faults and with experimental studies for deformation of rock types similar to those at Gubbio.

The displacements accommodated along F1–F4 are concentrated mostly along the PSSs themselves and also within the PSZs. The presence of fractured, sub-rounded clasts and ultrafine-grained gouge material suggests that cataclastic deformation occurred within the PSZs. The presence of SLZs < 20 µm wide, which themselves contain further shear surfaces and an increasing proportion of phyllosilicates, suggests that shear becomes progressively localised into narrower zones during slip evolution. Similar styles of shear localisation are observed in a number of experimental studies and associated with a transition from stable sliding (velocity-strengthening) to unstable, stick-slip (velocity-weakening) behaviour (e.g. Engelder et al., 1975; Moore et al., 1988; Logan et al., 1992; Beeler et al., 1996; Collettini et al., 2011; Ikari et al., 2011). These experiments were performed on a wide range of crustal rock types (quartz, calcite, quartzo-feldspathic and phyllosilicate gouges) and under a broad spectrum of experimental conditions. On this evidence, it seems possible that the PSSs F1–F4 have behaved in a velocity- and/or slip-weakening manner. This interpretation would be consistent with the fact that they are derived from the micritic limestone protolith, since carbonate rocks do experimentally exhibit both velocity- and slip-weakening behaviour under certain conditions. For example, Verberne et al. (2010) recorded a change from velocity-strengthening to velocity-weakening in limestone gouge at temperatures between 100 and 150 °C; Collettini et al. (2011) observed an evolution from velocity-strengthening to velocity-weakening with increasing sliding velocity; and Logan et al. (1992) observed this transition at confining pressures > 50 MPa.

In FD4, displacement is distributed throughout the domain with movement accommodated along pressure-solution seams in the S–C fabric. The common occurrence of slickenfibres on C-plane surfaces suggests that the shearing within this domain is fluid-assisted. The microstructures observed within the pressure-solution seams, such as folds and kinks of the phyllosilicates and pressure shadows around clasts, are indicative of bulk ductile flow by diffusive mass transfer. They are very similar to those reported by Holdsworth et al. (2011) and Hadizadeh et al. (2012) in the phyllosilicate-rich, actively creeping zone of the San Andreas fault, i.e. they are more typical of creeping deformation than seismic slip. Interpreting the structures in FD4 to be of aseismic origin

would be consistent with their phyllosilicate-rich composition due to the marly protolith, because phyllosilicates have been shown experimentally to be almost exclusively velocity-strengthening (e.g. Morrow et al., 2007; Tembe et al., 2010; Ikari et al., 2011 and references therein). The proportion of phyllosilicates within the solution seams is >50%, which experimental evidence suggests is enough for the frictional behaviour to be controlled by the weak phyllosilicates rather than by the stronger carbonate phases (e.g. Tesei et al., 2012), due to the formation of an interconnected clay network (e.g. Schleicher et al., 2010; Tembe et al., 2010). Although phyllosilicates comprise <20% of the rock volume in FD4, the fact that they are concentrated along the solution seams means that shear strain can preferentially be focused along these pre-existing zones of weakness (Collettini et al., 2009; Behnsen and Faulkner, 2012), so that ultimately, the strength and frictional behaviour of FD4 is likely dominated by the weak phyllosilicate-rich seams. Thus, we hypothesise that FD4 deforms predominantly in a velocity-strengthening, aseismic manner, with the potential to act as a barrier to rupture propagation (e.g. Boatwright and Cocco, 1996; Kaneko et al., 2010). Consequently, earthquake ruptures might tend to bypass FD4, and concentrate displacement along the PSSs F1–F4, which lie within the velocity-weakening, micritic limestone part of the fault core.

5.3. Coseismic slip indicators

As well as having the potential to exhibit velocity-weakening behaviour, carbonate rocks are also widely shown to demonstrate strong dynamic-weakening behaviour at seismic slip rates (>1 m/s), when the frictional strength of carbonate faults reduces dramatically from Byerlee values ($\mu = 0.6$–0.85) to values as low as 0.1 (Han et al., 2007, 2010, 2011; De Paola et al., 2011a; 2011b). The weakening mechanisms are thought to be thermally activated due to the frictional heat generated along highly localised slip surfaces during rapid seismic slip (Di Toro et al., 2011).

Temperatures attained within micron-scale width slip zones at seismic slip rates may be on the order of several hundreds of degrees Celsius and that would be sufficient to trigger physical and chemical modifications to the fault rocks and slip-zone materials. For example, in carbonates, these conditions can trigger decarbonation reactions, releasing CO_2 gas into the slip zone and producing a thin layer of sub-rounded and spherical nanoparticles of lime (CaO) within the slip zone. These nanoparticles may be able to undergo rolling along the slip surface, leading to fault lubrication (Han et al., 2010, 2011; De Paola et al., 2011a).

As described in Section 3.4.2, within one of the SLZs present within the PSZ of F4, we observed bubble-like features set within a matrix of elongate calcite crystals and phyllosilicate, together with some unusual “dog-bone” or “H”-shaped calcite crystals. These microstructures are strikingly similar to those observed by Collettini et al. (2013) within the PSZ of the Spoleto thrust in central Italy. Collettini et al. (2013) performed transmission electron microscope analyses on the matrix material within the PSZ and found the presence of amorphous silicate. The fault rocks at Spoleto are derived from the Scaglia Rossa Formation, so they are formed from the same protolith as the fault rocks at Gubbio and also formed at similar depths of 2–3 km. Collettini et al. (2013) suggested that the observed microstructures are produced by thermally-triggered reactions in the PSZ as a result of rapid heating during earthquake slip. They propose that dehydroxylation of clays has resulted in amorphisation, and that the skeletal habit of calcite is a result of disequilibrium crystallisation under rapid cooling conditions (e.g. Faure et al., 2003) following carbonate dissociation. The fact that we can make a direct comparison between the microstructures observed along F4 and those described above of Collettini et al. (2013) leads to the conclusion that F4 has slipped coseismically.

The absence of smectite in the PSZs of F1–F4, as revealed by XRD analyses, may also be due to frictional heating associated with seismic slip, since smectite becomes unstable at temperatures between 120 and 150 °C and collapses to an illite-type structure (e.g. Pytte and Reynolds, 1989). The exact mechanism of this smectite-illite transformation has not been well constrained, but it is often associated with the loss of interlayer water (due to dehydration) (Colten-Bradley, 1987).

With knowledge of the thickness of the PSZ, the thermal properties of the PSZ constituents, plus the slip rates and displacements experienced during a seismic event of a given magnitude, it is possible to estimate the average temperature attained within the PSZ during the propagation of an earthquake. Given that the SLZs present within the PSZs are on the order of <20 μm wide, we can simplify our analysis to assume that slip occurred within a zone of zero thickness (Rice, 2006), making it possible to use the equation of Carslaw and Jaeger (1959) to estimate the temperature rise:

$$T_{Av} = \frac{\tau_{av}\sqrt{Dv}}{\rho c_p \sqrt{\pi k}} \quad (1)$$

where D = displacement (using values of earthquake slip for a given magnitude as presented by Sibson, 1989), τ_{av} = the shear strength of the fault for a hydrostatic fluid pressure of $\lambda = 0.4$, v = slip velocity, and ρ, c_p and κ are the density, specific heat capacity and thermal diffusivity, respectively, of the slip zone materials. We use values for calcite of $\rho = 2710\ \mathrm{kg\,m^{-3}}$, $c_p = 820\ \mathrm{J\,kg^{-1}\,K^{-1}}$ and $\kappa = 1.62 \times 10^{-6}\ \mathrm{m^2\,s^{-1}}$ (Wangen, 2010), values for smectite of $\rho = 2608\ \mathrm{kg\,m^{-3}}$, $c_p = 795\ \mathrm{J\,kg^{-1}\,K^{-1}}$ and $\kappa = 0.91 \times 10^{-6}\ \mathrm{m^2\,s^{-1}}$ (Wangen, 2010) and values for illite of $\rho = 2660\ \mathrm{kg\,m^{-3}}$, $c_p = 808\ \mathrm{J\,kg^{-1}\,K^{-1}}$ and $\kappa = 0.86 \times 10^{-6}\ \mathrm{m^2\,s^{-1}}$ (Wangen, 2010). Considering a depth of faulting of 2.5 km, this equation yields temperatures adequate for calcite decarbonation, which initiates at a temperature of ~720 °C (Sharp et al., 2003), for earthquakes with $M > 3$, in the case of a strong fault ($\mu = 0.85$), or $M > 6$, in the case of a weak fault ($\mu = 0.2$). Dehydroxylation of smectite and illite initiate at temperatures of approximately 600 °C (Shoval, 2003) and 900 °C (Jordán et al., 1999) respectively. This behaviour would correspond to an $M > 3$ earthquake in the case of a strong fault, and an $M > 5$ earthquake in the case of a weak fault. Thus, the historical normal-faulting earthquakes that have occurred throughout the Apennines, which typically have $M \approx 5$–6, could easily trigger thermal decomposition reactions and leave behind recrystallised calcite textures and clay transformations as signatures of seismic slip.

We have also observed nanoparticles coating the slip surfaces of F1–F4 (Section 3.4.2.2; Fig. 9e and f), providing further evidence that the thermal dissociation of carbonate may have occurred and that dynamic weakening was operative along these faults. In fact, their tightly-packed geometries and polygonal boundaries resemble those produced experimentally by Smith et al. (2013), who suggested that they result from dynamic recrystallisation due to intense frictional heating. Thus, there are several lines of

Table 1
Summary of clay fraction XRD results. Percentages are estimates based on peak area.

Sample #	Description	Illite	Smectite	Kaolinite
2	Protolith (micritic limestone)	6.15%	93.20%	0.64%
28	Protolith (marly limestone)	11.70%	87.60%	0.70%
21a	Solution seam (FD3)	79.60%	15.80%	4.60%
28 (2010)	Solution seam (FD4)	45.54%	28.60%	25.85%
10	PSZ (F3)	92.60%	0.00%	7.40%
21b	PSZ (F4)	84.60%	2.00%	13.40%

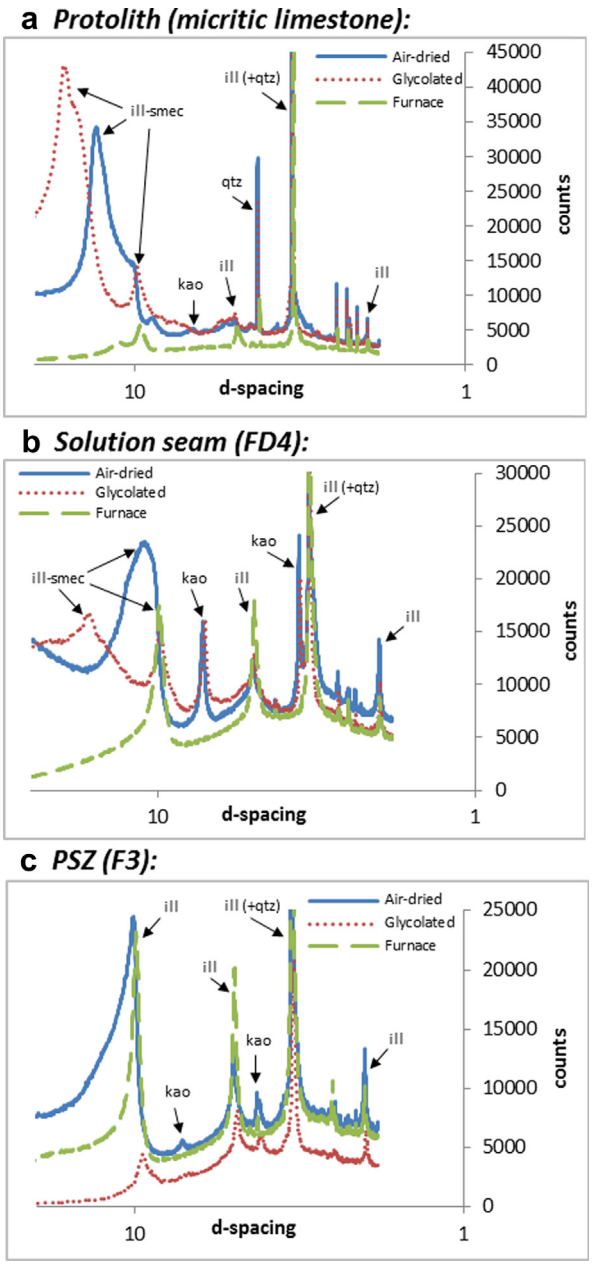

Fig. 11. Representative XRD traces of the clay fraction present in different parts of the fault zone: a) The micritic limestone protolith. b) A pressure-solution seam from FD4. c) A PSZ from F3. See Table 1 for a summary of the results and see text for discussion. (ill-smec = mixed-layer illite-smectite; kao = kaolinite; ill = illite; qtz = quartz).

evidence to suggest that seismic slip has occurred along the PSSs F1–F4, but we have been unable to identify any seismic signatures within domain FD4, further supporting our hypothesis that FD4 behaves predominantly aseismically.

5.4. Seismic vs. aseismic behaviour during the seismic cycle

While it would be useful if our hypothesis fully described the deformation behaviour of the fault core, evidence suggests that the simple seismic vs. aseismic differentiation between the PSSs F1–F4 and domain FD4 is unlikely. Firstly, carbonate rocks do not behave exclusively in a velocity-weakening manner (Logan et al., 1992; Verberne et al., 2010; Collettini et al., 2011) and shear localisation is not always associated with stick-slip behaviour (e.g. Logan et al., 1979; Marone et al., 1990; Rathbun and Marone, 2010). Similarly, phyllosilicates do not behave exclusively in a velocity-strengthening manner (e.g. Saffer and Marone, 2003; Ikari et al., 2007; Niemeijer et al., 2012). Frictional behaviour is dependent on a number of factors, including the ambient conditions (normal stress, temperature and pore fluid pressure), the imposed rupture velocity, pre-existing structures within the slip zone, and the composition and distribution of mineral phases within the slip zone.

Secondly, Kaneko et al. (2010) showed that under certain conditions, velocity-strengthening fault patches can host earthquake ruptures, for example, if the earthquake is of large-enough magnitude to overcome the negative stress drop encountered within the velocity-strengthening material, or because of high pre-stress in the velocity-strengthening patch as a consequence of it not being ruptured during previous seismic events. This would explain the occurrence of a localised zone of shearing in the centre of FD4. Indeed, once transected, seismic ruptures may exploit this localised zone in FD4 by reactivation.

A complex interplay between seismic and aseismic behaviour is also evident from our microstructural observations. For example, we have observed that many slip surfaces associated with F1–F4 have stylolitic morphologies, highlighted by the presence of phyllosilicate (Section 3.4.2; Fig. 8e and d). We have also observed SLZs that are enriched in phyllosilicates (up to 80%; Fig. 9a). The concentration of phyllosilicates within PSZs is likely to be a result of pressure-solution processes operating along the PSSs during the interseismic period. And thus at certain times during the seismic cycle, diffusive mass transfer processes dominate over cataclasis and frictional sliding within the PSZs. In fact, grain-size reduction by cataclasis will promote diffusive mass transfer processes and may lead to a transition from frictional to frictional-viscous behaviour (Bos and Spiers, 2001), therefore promoting fault creep. Conversely, the dissolution of the asperities along a fault surface may reduce their strength, causing them to break successively and trigger fracturing of the fault plane (Gratier and Gamond, 1990).

Finally, the variations in calcite vein textures observed within the PSZ of F3 (Section 3.4.2.2; Fig. 8b and d) further point to variations in the seismic history of the fault. As proposed by Gratier and Gamond (1990), a crack-seal texture (Ramsay, 1980) may reflect sliding occurring at a very slow rate, during which successive microcracks are healed. The presence of small euhedral crystals, on the other hand, may reflect precipitation of calcite into larger fluid-filled cavities created during more rapid displacement events (Gratier and Gamond, 1990), whilst the PSS-parallel stylolites are indicative of fault healing by pressure-solution welding (e.g. Yasuhara et al., 2005).

Despite these complexities, we propose a simplified conceptual model, which summarises possible scenarios for the mechanical behaviour of the Gubbio fault (Fig. 12). During an earthquake, the micritic limestone-dominated portions of the fault core accommodate the coseismic displacements along the localised PSSs F1–F4. This localisation is accompanied by fracturing and/or hydrofracturing within domains FD1–FD3. At these times, domain FD4, which does not accommodate either of these modes of deformation, remains loaded, and this residual stress is then relaxed during the post-seismic period by slow, creeping afterslip deformation concentrated in the marly sections of the fault core. Alternatively, it may be that domain FD4 and certain parts of domains FD1–FD3, i.e. the pressure-solution seams, and certain portions of the PSZs of F1–F4, creep continuously during the interseismic period, whilst the other parts of the fault core remain locked. This behaviour will increase the stresses in the locked parts of the fault core until they fail seismogenically. In addition, Sagi (2012) found that the marl-rich units of the Scaglia Rossa Formation act as fault seals, inhibiting fluid flow. This

behaviour is consistent with the observation that calcite veining in FD4 occurs to a much lesser extent than in domains FD1–FD3. It is possible that the fluids involved in the pressure-solution processes in FD4, transport material away from FD4 to be deposited in the veins within FD1–FD3. Either way, the preferential transport of fluids away from FD4 and towards FD1–FD3 will generate a fluid overpressure and result in the hydrofracturing and hydraulic brecciation that we observe in domains FD1–FD3. This fluid overpressure can also trigger seismic slip along the PSSs F1–F4, which would be consistent with the fact that some PSZs are characterised by calcite veining (e.g. Fig. 5d) and chaotic breccias (e.g. Fig. 5b). A similar mixed-mode fault slip behaviour has been proposed, and supported experimentally, by Collettini et al. (2011) for the Zuccale fault zone, which similarly consists of domains of competent carbonate material surrounded by foliated, phyllosilicate-rich horizons (Collettini and Holdsworth, 2004; Collettini et al., 2011).

Although there is no recorded evidence of afterslip deformation occurring at Gubbio specifically, one of the best-documented examples of afterslip deformation comes from L'Aquila, ~130 km south of Gubbio, after the 2009 Mw 6.1 earthquake, where post-seismic deformation may have amounted to as much as 50% of the coseismic slip (Wilkinson et al., 2010; D'Agostino et al., 2012). Evidence of interseismic creep in the Apennines is also limited, but D'Agostino et al. (2009) identified, through the study of GPS velocity fields, a significant deficit in seismic release in the Umbria–Marche Apennines, which makes aseismic activity a real possibility. The one place where interseismic creep is documented in the northern Apennines is along the Alto-Tiberina low-angle normal fault, of which the Gubbio fault is an antithetic splay (Chiaraluce et al., 2007; Hreinsdóttir and Bennett, 2009). These observations show that the lithologies through which the Gubbio fault penetrates are able to accommodate aseismic creep. The driving forces and mechanisms by which afterslip and interseismic creep occur are not yet fully understood, but a number of recent studies show a coincidence between the operation of pressure-solution creep and the aseismic sliding of active faults (Gratier et al., 2011, 2013; Holdsworth et al., 2011; Hadizadeh et al., 2012).

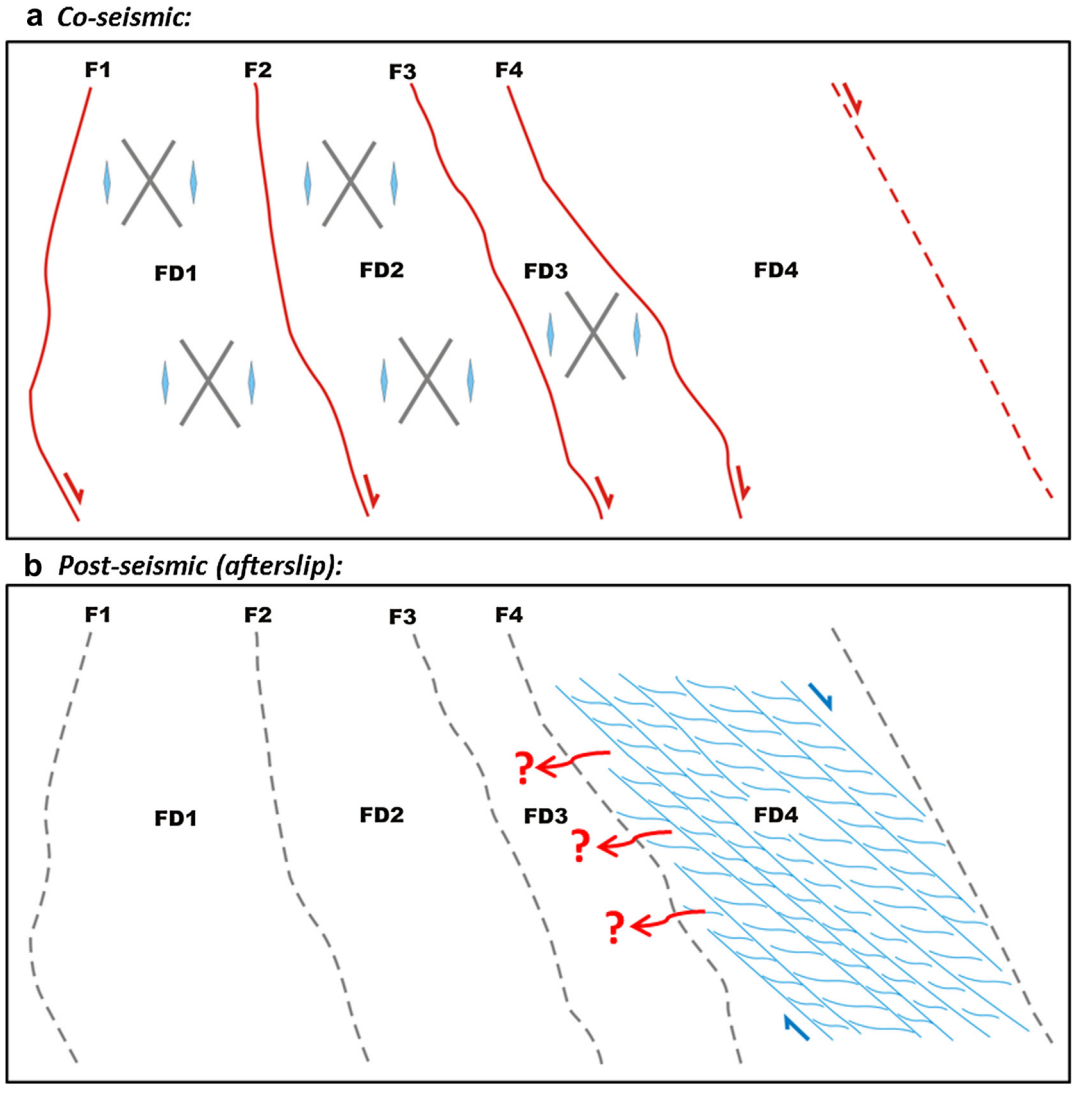

Fig. 12. A conceptual model summarising our proposed behaviour of the Gubbio fault over the course of the seismic cycle. a) During the coseismic period, activity is concentrated within the micritic limestone-hosted parts of the fault core. Coseismic displacements are localised along the PSSs F1–F4 and seismic energy dissipated through domains FD1–FD3 produces fractures/hydrofractures, resulting in extensive brecciation over time within these domains. FD4 remains locked during the coseismic period due to its velocity-strengthening nature, resulting in stress accumulation within the domain. b) During the post-seismic period, the accumulated stress in FD4 is relaxed by slow, creeping afterslip deformation. If FD4 creeps continuously during the interseismic period, stress in the locked domains FD1–FD3 will increase, until they fail seismogenically. The possible transfer of fluids away from FD4, as shown by the red arrows, may further enhance stress accumulation in domains FD1–FD3.

Other factors besides lithology can control the distribution of seismicity within a fault zone such as geometric complexities, which can induce different strain rates within a fault zone (e.g. Tesei et al., 2013), and the location of the mainshock rupture patch, since post-seismic strains will preferentially occur in the areas surrounding the location of the mainshock (e.g. Johnson et al., 2006; Ozawa et al., 2011; D'Agostino et al., 2012). But still, playing down the importance of lithology is hard in these cases. Geometric complexities within fault zones are often a result of lithological heterogeneities within the sequences through which a fault traverses (e.g. Bonson et al., 2007; Nemser and Cowan, 2009; Tesei et al., 2013). Also, lithology can control the location of earthquake rupture patches, since, as discussed in Section 5.2, earthquakes will only nucleate in materials that are velocity-weakening.

6. Conclusion

The majority of displacement at the Cava Filippi outcrop is accommodated along the PSSs F1–F4 and in domain FD4. Along F1–F4, the dominant deformation mechanisms are cataclasis and frictional sliding. The resulting microstructures and localised deformation features are similar to those observed in both natural and experimental examples of major earthquake-hosting faults. We therefore propose that earthquake nucleation and propagation are favoured along F1–F4, which are hosted in micritic limestones. Domain FD4 is characterised by continuous, distributed deformation with the dominant deformation mechanism being pressure-solution. The structures observed in FD4 are comparable to those observed in natural and experimental examples of creeping faults. Thus, we propose that domain FD4 behaves in an aseismic manner and we attribute this behaviour to its phyllosilicate-rich host rock. The behaviour of the Gubbio fault over the course of the seismic cycle is therefore likely to be complex, with a lithologically-controlled interplay between localised earthquake nucleation and propagation, and distributed interseismic and post-seismic deformation. Combined field, microstructural, geodetic and experimental studies of faults in varying lithologies, and under a range of conditions, will help us to better constrain the role of lithology in controlling fault behaviour, so that lithological variations along or across a fault may be considered when assessing the past seismicity and future seismic hazard of a fault.

Acknowledgements

We thank Cristiano Collettini and an anonymous reviewer for thoughtful comments which helped to improve the manuscript. Thanks also go to the Editor, William Dunne, for further constructive revisions. This work was funded by the Natural Environment Research Council through a NERC PhD studentship NE/J500215/1 awarded to RJB, and a NERC Standard Grant NE/H021744/1 awarded to NDP. L. Bowen (G.J. Russell Microscopy Facility, Durham University, UK) provided assistance during SEM analyses. We thank also E. Dempsey and I. Faoro for assistance in the field. Enquiries regarding access to research materials should be directed towards the corresponding author.

References

Agosta, F., Aydin, A., 2006. Architecture and deformation mechanism of a basin-bounding normal fault in Mesozoic platform carbonates, central Italy. J. Struct. Geol. 28, 1445–1467.

Amato, A., Azzara, R., Chiarabba, C., Cimini, G., Cocco, M., Di Bona, M., Margheriti, L., Mazza, S., Mele, F., Selvaggi, G., 1998. The 1997 Umbria–Marche, Italy, earthquake sequence: a first look at the main shocks and aftershocks. Geophys. Res. Lett. 25, 2861–2864.

Barchi, M., DeFeyter, A., Magnani, M., Minelli, G., Pialli, G., Sotera, B., 1998a. Extensional tectonics in the northern Apennines (Italy): evidence from the CROP03 deep seismic reflection line. Mem. Soc. Geol. Ital. 52, 528–538.

Barchi, M., DeFeyter, A., Magnani, M., Minelli, G., Pialli, G., Sotera, B., 1998b. The structural style of the Umbria–Marche fold and thrust belt. Mem. Soc. Geol. Ital. 52, 557–578.

Barchi, M., Pucci, S., Collettini, C., Mirabella, F., Massoli, D., Guzzetti, F., Reichenbach, P., Cardinali, M., Vergoni, N., Troiani, E., Chiraz, P., Giombini, L., 2001. A geologic map of the Colfiorito area. Geoitalia, 333–334, 3° forum first poster session.

Bastesen, E., Braathen, A., 2010. Extensional faults in fine grained carbonates – analysis of fault core lithology and thickness–displacement relationships. J. Struct. Geol. 32, 1609–1628.

Beeler, N., Tullis, T., Blanpied, M., Weeks, J., 1996. Frictional behavior of large displacement experimental faults. J. Geophys. Res. 101, 8697–8715.

Behnsen, J., Faulkner, D.R., 2012. The effect of mineralogy and effective normal stress on frictional strength of sheet silicates. J. Struct. Geol. 42, 49–61.

Boatwright, J., Cocco, M., 1996. Frictional constraints on crustal faulting. J. Geophys. Res.: Solid Earth 101, 13895–13909.

Boncio, P., Brozzetti, F., Ponziani, F., Barchi, M., Lavecchia, G., Pialli, G., 1998. Seismicity and extensional tectonics in the northern Umbria–Marche Apennines. Mem. Geol. Soc. Italy 52, 539–555.

Boncio, P., Lavecchia, G., 2000. A structural model for active extension in central Italy. J. Geodyn. 29, 233–244.

Bonson, C.G., Childs, C., Walsh, J.J., Schöpfer, M.P., Carboni, V., 2007. Geometric and kinematic controls on the internal structure of a large normal fault in massive limestones: the Maghlaq Fault, Malta. J. Struct. Geol. 29, 336–354.

Bortolotti, V., Passerini, P., Sagri, M., Sestini, G., 1970. The miogeosynclinal sequences. Sediment. Geol. 4, 341–444.

Bos, B., Spiers, C., 2001. Experimental investigation into the microstructural and mechanical evolution of phyllosilicate-bearing fault rock under conditions favouring pressure solution. J. Struct. Geol. 23, 1187–1202.

Burkhard, M., 1993. Calcite twins, their geometry, appearance and significance as stress-strain markers and indicators of tectonic regime: a review. J. Struct. Geol. 15, 351–368.

Bussolotto, M., Benedicto, A., Invernizzi, C., Micarelli, L., Plagnes, V., Deiana, G., 2007. Deformation features within an active normal fault zone in carbonate rocks: the Gubbio fault (Central Apennines, Italy). J. Struct. Geol. 29, 2017–2037.

Byerlee, J., 1978. Friction of rocks. Pure Appl. Geophys. 116, 615–626.

Carslaw, H., Jaeger, J., 1959. Conduction of Heat in Solids, second ed. Oxford University Press, New York.

Carpenter, B., Marone, C., Saffer, D., 2011. Weakness of the San Andreas Fault revealed by samples from the active fault zone. Nature Geoscience 4, 251–254.

Chester, F., Logan, J., 1986. Implications for mechanical properties of brittle faults from observations of the Punchbowl fault zone, California. Pure Appl. Geophys. 124, 79–106.

Chester, F.M., Evans, J.P., Biegel, R.L., 1993. Internal structure and weakening mechanisms of the San Andreas Fault. J. Geophys. Res. 98, 771–786.

Chester, F.M., Chester, J.S., 1998. Ultracataclasite structure and friction processes of the Punchbowl fault, San Andreas system, California. Tectonophysics 295, 199–221.

Chiarabba, C., et al., 2009. The 2009 L'Aquila (central Italy) Mw6. 3 earthquake: main shock and aftershocks. Geophys. Res. Lett. 36, L18308. http://dx.doi.org/10.1029/2009GL039627.

Chiaraluce, L., 2012. Unravelling the complexity of Apenninic extensional fault systems: a review of the 2009 L'Aquila earthquake (Central Apennines, Italy). J. Struct. Geol. 42, 2–18.

Chiaraluce, L., Chiarabba, C., Collettini, C., Piccinini, D., Cocco, M., 2007. Architecture and mechanics of an active low-angle normal fault: Alto Tiberina Fault, northern Apennines, Italy. J. Geophys. Res. 112, B10310. http://dx.doi.org/10.1029/2007JB005015.

Collettini, C., Barchi, M., Chiaraluce, L., Mirabella, F., Pucci, S., 2003. The Gubbio fault: can different methods give pictures of the same object? J. Geodyn. 36, 51–66.

Collettini, C., Holdsworth, R., 2004. Fault zone weakening and character of slip along low-angle normal faults: insights from the Zuccale fault, Elba, Italy. J. Geol. Soc. 161, 1039–1051.

Collettini, C., Niemeijer, A., Viti, C., Marone, C., 2009. Fault zone fabric and fault weakness. Nature 462, 907–910.

Collettini, C., Niemeijer, A., Viti, C., Smith, S.A.F., Marone, C., 2011. Fault structure, frictional properties and mixed-mode fault slip behavior. Earth Planet. Sci. Lett. 311, 316–327.

Collettini, C., Viti, C., Tesei, T., Mollo, S., 2013. Thermal decomposition along natural carbonate faults during earthquakes. Geology 41, 927–930.

Colten-Bradley, V.A., 1987. Role of pressure in smectite dehydration – effects on geopressure and smectite-to-illite transformation. AAPG Bull. 71, 1414–1427.

D'Agostino, N., Cheloni, D., Fornaro, G., Giuliani, R., Reale, D., 2012. Space-time distribution of afterslip following the 2009 L'Aquila earthquake. J. Geophys. Res. 117, B02402. http://dx.doi.org/10.1029/2011JB008523.

D'Agostino, N., Mantenuto, S., D'Anastasio, E., Avallone, A., Barchi, M., Collettini, C., Radicioni, F., Stoppini, A., Fastellini, G., 2009. Contemporary crustal extension in the Umbria–Marche Apennines from regional CGPS networks and comparison between geodetic and seismic deformation. Tectonophysics 476, 3–12.

De Paola, N., Chiodini, G., Hirose, T., Cardellini, C., Caliro, S., Shimamoto, T., 2011a. The geochemical signature caused by earthquake propagation in carbonate-hosted faults. Earth Planet. Sci. Lett. 310, 225–232.
De Paola, N., Collettini, C., Faulkner, D., Trippetta, F., 2008. Fault zone architecture and deformation processes within evaporitic rocks in the upper crust. Tectonics 27, TC4017. http://dx.doi.org/10.1029/2007TC002230.
De Paola, N., Hirose, T., Mitchell, T., Di Toro, G., Viti, C., Shimamoto, T., 2011b. Fault lubrication and earthquake propagation in thermally unstable rocks. Geology 39, 35–38.
De Paola, N., Mirabella, F., Barchi, M., Burchielli, F., 2006. Early orogenic normal faults and their reactivation during thrust belt evolution: the Gubbio fault case study, Umbria–Marche Apennines (Italy). J. Struct. Geol. 28, 1948–1957.
Deschamps, A., Iannaccone, G., Scarpa, R., 1984. The Umbrian earthquake (Italy) of 19 September 1979. Ann. Geophys. 2, 29–36.
Di Toro, G., Han, R., Hirose, T., De Paola, N., Nielsen, S., Mizoguchi, K., Ferri, F., Cocco, M., Shimamoto, T., 2011. Fault lubrication during earthquakes. Nature 471, 494–498.
Dieterich, J.H., Kilgore, B.D., 1994. Direct observation of frictional contacts: new insights for state-dependent properties. Pure Appl. Geophys. 143, 283–302.
Dziewonski, A., Franzen, J., Woodhouse, J., 1985. Centroid-moment tensor solutions for April–June, 1984. Phys. Earth Planet. Inter. 37, 87–96.
Ekström, G., Morelli, A., Boschi, E., Dziewonski, A.M., 1998. Moment tensor analysis of the central Italy earthquake sequence of September–October 1997. Geophys. Res. Lett. 25, 1971–1974.
Engelder, J.T., Logan, J.M., Handin, J., 1975. The sliding characteristics of sandstone on quartz fault-gouge. Pure Appl. Geophys. 113, 69–86.
Fagereng, Å., Sibson, R.H., 2010. Melange rheology and seismic style. Geology 38, 751–754.
Faulkner, D., Lewis, A., Rutter, E., 2003. On the internal structure and mechanics of large strike-slip fault zones: field observations of the Carboneras fault in southeastern Spain. Tectonophysics 367, 235–251.
Faulkner, D., Jackson, C., Lunn, R., Schlische, R., Shipton, Z., Wibberley, C., Withjack, M., 2010. A review of recent developments concerning the structure, mechanics and fluid flow properties of fault zones. J. Struct. Geol. 32, 1557–1575.
Faure, F., Trolliard, G., Nicollet, C., Montel, J.-M., 2003. A developmental model of olivine morphology as a function of the cooling rate and the degree of under-cooling. Contrib. Mineral. Petrol. 145, 251–263.
Fondriest, M., Smith, S.A.F., Di Toro, G., Zampieri, D., Mittempergher, S., 2012. Fault zone structure and seismic slip localization in dolostones, an example from the Southern Alps, Italy. J. Struct. Geol. 45, 52–67.
GE.MI.NA, 1963. Ligniti e torbe dell'Italia Centrale. GE.MI.NA., Geomineraria Nazionale, Torino.
Gratier, J., Gamond, J., 1990. Transition between seismic and aseismic deformation in the upper crust. Geol. Soc., Lond., Spec. Publ. 54, 461–473.
Gratier, J.-P., Richard, J., Renard, F., Mittempergher, S., Doan, M.-L., Di Toro, G., Hadizadeh, J., Boullier, A.-M., 2011. Aseismic sliding of active faults by pressure solution creep: evidence from the San Andreas Fault Observatory at Depth. Geology 39, 1131–1134.
Gratier, J.P., Thouvenot, F., Jenatton, L., Tourette, A., Doan, M.L., Renard, F., 2013. Geological control of the partitioning between seismic and aseismic sliding behaviours in active faults: evidence from the Western Alps, France. Tectonophysics 600, 226–242.
Gu, Y., Wong, T., 1994. Development of shear localization in simulated quartz gouge: effect of cumulative slip and gouge particle size. Pure Appl. Geophys. 143, 387–423.
Hadizadeh, J., Mittempergher, S., Gratier, J.P., Renard, F., Di Toro, G., Richard, J., Babaie, H.A., 2012. A microstructural study of fault rocks from the SAFOD: implications for the deformation mechanisms and strength of the creeping segment of the San Andreas Fault. J. Struct. Geol. 42, 246–260.
Haessler, H., Gaulon, R., Rivera, L., Console, R., Frogneux, M., Gasparini, G., Martel, L., Patau, G., Siciliano, M., Cisternas, A., 1988. The Perugia (Italy) earthquake of 29, April 1984: a microearthquake survey. Bull. Seismol. Soc. Am. 78, 1948–1964.
Han, R., Hirose, T., Shimamoto, T., 2010. Strong velocity weakening and powder lubrication of simulated carbonate faults at seismic slip rates. J. Geophys. Res. 115, B03412. http://dx.doi.org/10.1029/2008JB006136.
Han, R., Hirose, T., Shimamoto, T., Lee, Y., Ando, J., 2011. Granular nanoparticles lubricate faults during seismic slip. Geology 39, 599–602.
Han, R., Shimamoto, T., Hirose, T., Ree, J.H., Ando, J., 2007. Ultralow friction of carbonate faults caused by thermal decomposition. Science 316, 878–881.
Holdsworth, R., Van Diggelen, E., Spiers, C., De Bresser, J., Walker, R., Bowen, L., 2011. Fault rocks from the SAFOD core samples: implications for weakening at shallow depths along the San Andreas Fault, California. J. Struct. Geol. 33, 132–144.
Hreinsdóttir, S., Bennett, R.A., 2009. Active aseismic creep on the Alto Tiberina low-angle normal fault, Italy. Geology 37, 683–686.
Ikari, M.J., Marone, C., Saffer, D.M., 2011. On the relation between fault strength and frictional stability. Geology 39, 83–86.
Ikari, M.J., Saffer, D.M., Marone, C., 2007. Effect of hydration state on the frictional properties of montmorillonite-based fault gouge. J. Geophys. Res. 112, B06423. http://dx.doi.org/10.1029/2006JB004748.
Ikari, M.J., Saffer, D.M., Marone, C., 2009. Frictional and hydrologic properties of clay-rich fault gouge. J. Geophys. Res. 114, B05409. http://dx.doi.org/10.1029/2008JB006089.
ISC, 2001. On-line Bulletin. International Seismological Centre, Thatcham, United Kingdom. http://www.isc.ac.uk, 2011.
Jefferies, S.P., Holdsworth, R.E., Wibberley, C.A.J., Shimamoto, T., Spiers, C.J., Niemeijer, A.R., Lloyd, G.E., 2006. The nature and importance of phyllonite development in crustal-scale fault cores: an example from the Median Tectonic Line, Japan. J. Struct. Geol. 28, 220–235.
Johnson, K.M., Bürgmann, R., Larson, K., 2006. Frictional properties on the San Andreas Fault near Parkfield, California, inferred from models of afterslip following the 2004 earthquake. Bull. Seismol. Soc. Am. 96, S321–S338.
Jordán, M.M., Boix, A., Sanfeliu, T., de la Fuente, C., 1999. Firing transformations of cretaceous clays used in the manufacturing of ceramic tiles. Appl. Clay Sci. 14, 225–234.
Kaneko, Y., Avouac, J.-P., Lapusta, N., 2010. Towards inferring earthquake patterns from geodetic observations of interseismic coupling. Nat. Geosci. 3, 363–369.
Kuo, L.-W., Hsiao, H.-C., Song, S.-R., Sheu, H.-S., Suppe, J., 2013. Coseismic thickness of principal slip zone from the Taiwan Chelungpu fault Drilling Project-A (TCDP-A) and correlated fracture energy. Tectonophysics in press.
Li, H., Wang, H., Xu, Z., Si, J., Pei, J., Li, T., Huang, Y., Song, S.-R., Kuo, L.-W., Sun, Z., 2013. Characteristics of the fault-related rocks, fault zones and the principal slip zone in the Wenchuan Earthquake Fault Scientific Drilling Project Hole-1 (WFSD-1). Tectonophysics 584, 23–42.
Lockner, D.A., Morrow, C., Moore, D., Hickman, S., 2011. Low strength of deep San Andreas Fault gouge from SAFOD core. Nature 472, 82–85.
Logan, B.W., Semeniuk, V., 1976. Dynamic Metamorphism: Processes and Products in Devonian Carbonate Rocks, Canning Basin, Western Australia. Geological Society of Australia.
Logan, J., Friedman, M., Higgs, N., Dengo, C., Shimamoto, T., 1979. Experimental Studies of Simulated Gouge and Their Application to Studies of Natural Fault Zones: Analyses of Actual Fault Zones in Bedrock. United States geological survey open file report 1239, pp. 305–343.
Logan, J., Dengo, C., Higgs, N., Wang, Z., 1992. Fabrics of experimental fault zones: their development and relationship to mechanical behavior. Int. Geophys. Ser. 51, 33.
Marone, C., 1998. Laboratory-derived friction laws and their application to seismic faulting. Annu. Rev. Earth Planet. Sci. 26, 643–696.
Marone, C., Raleigh, C.B., Scholz, C., 1990. Frictional behavior and constitutive modeling of simulated fault gouge. J. Geophys. Res. 95, 7007–7025.
Micarelli, L., Benedicto, A., Wibberley, C., 2006. Structural evolution and permeability of normal fault zones in highly porous carbonate rocks. J. Struct. Geol. 28, 1214–1227.
Mirabella, F., Ciaccio, M., Barchi, M., Merlini, S., 2004. The Gubbio normal fault (central Italy): geometry, displacement distribution and tectonic evolution. J. Struct. Geol. 26, 2233–2249.
Molli, G., Cortecci, G., Vaselli, L., Ottria, G., Cortopassi, A., Dinelli, E., Mussi, M., Barbieri, M., 2010. Fault zone structure and fluid–rock interaction of a high angle normal fault in Carrara marble (NW Tuscany, Italy). J. Struct. Geol. 32, 1334–1348.
Moore, D., Summers, R., Byerlee, J., 1988. Relationship between textures and sliding motion of experimentally deformed fault gouge: application to fault zone behavior. In: The 29th US Symposium on Rock Mechanics (USRMS).
Moore, D.E., Lockner, D.A., 2004. Crystallographic controls on the frictional behavior of dry and water-saturated sheet structure minerals. J. Geophys. Res. 109, B03401. http://dx.doi.org/10.1029/2003JB002582.
Moore, D.E., Lockner, D.A., 2011. Frictional strengths of talc-serpentine and talc-quartz mixtures. J. Geophys. Res. 116, B01403. http://dx.doi.org/10.1029/2010JB007881.
Morrow, C., Solum, J., Tembe, S., Lockner, D., Wong, T.F., 2007. Using drill cutting separates to estimate the strength of narrow shear zones at SAFOD. Geophys. Res. Lett. 34, L11301. http://dx.doi.org/10.1029/2007GL029665.
Nemser, E.S., Cowan, D.S., 2009. Downdip segmentation of strike-slip fault zones in the brittle crust. Geology 37, 419–422.
Niemeijer, A., Collettini, C., Smith, S.A.F., Spiers, C.J., 2012. Frictional properties of Zuccale fault rocks from room temperature to in-situ conditions: results from high strain rotary shear experiments. Geophys. Res. Abstr. 14. EGU2012-8001.
Otsuki, K., Monzawa, N., Nagase, T., 2003. Fluidization and melting of fault gouge during seismic slip: identification in the Nojima fault zone and implications for focal earthquake mechanisms. J. Geophys. Res. 108 (B4), 2192. http://dx.doi.org/10.1029/2001JB001711.
Ozawa, S., Nishimura, T., Suito, H., Kobayashi, T., Tobita, M., Imakiire, T., 2011. Coseismic and postseismic slip of the 2011 magnitude-9 Tohoku-Oki earthquake. Nature 475, 373–376.
Piccinini, D., Cattaneo, M., Chiarabba, C., Chiaraluce, L., De Martin, M., Di Bona, M., Moretti, M., Selvaggi, G., Augliera, P., Spallarossa, D., 2003. A microseismic study in a low seismicity area of Italy: the Città di Castello 2000–2001 experiment. Ann. Geophys. 46, 1315–1324.
Pucci, S., De Martini, P.M., Pantosti, D., Valensise, G., 2003. Geomorphology of the Gubbio basin (central Italy): understanding the active tectonics and earthquake potential. Ann. Geophys. 46, 837–864.
Power, W.L., Tullis, T.E., 1989. The relationship between slickenside surfaces in fine-grained quartz and the seismic cycle. J. Struct. Geol. 11, 879–893.
Pytte, A., Reynolds, R., 1989. The thermal transformation of smectite to illite. Therm. Hist. Sediment. Basins: Methods Case Hist., 133–140.
Ramsay, J.G., 1980. The crack-seal mechanism of rock deformation. Nature 284, 135–139.
Rathbun, A.P., Marone, C., 2010. Effect of strain localization on frictional behavior of sheared granular materials. J. Geophys. Res. 115, B01204. http://dx.doi.org/10.1029/2009JB006466.

Rice, J.R., 2006. Heating and weakening of faults during earthquake slip. J. Geophys. Res. 111, B05311. http://dx.doi.org/10.1029/2005JB004006.
Rutter, E., 1976. The kinetics of rock deformation by pressure solution. Philos. Trans. R. Soc. Lond. Ser. A, Math. Phys. Sci. 283, 203–219.
Rutter, E., Maddock, R., Hall, S., White, S., 1986. Comparative microstructures of natural and experimentally produced clay-bearing fault gouges. Pure Appl. Geophys. 124, 3–30.
Rutter, E., Faulkner, D., Burgess, R., 2012. Structure and geological history of the Carboneras fault zone, SE Spain: part of a stretching transform fault system. J. Struct. Geol. 45, 68–86.
Rybacki, E., Evans, B., Janssen, C., Wirth, R., Dresen, G., 2013. Influence of stress, temperature, and strain on calcite twins constrained by deformation experiments. Tectonophysics 601, 20–36.
Saffer, D.M., Frye, K.M., Marone, C., Mair, K., 2001. Laboratory results indicating complex and potentially unstable frictional behavior of smectite clay. Geophys. Res. Lett. 28, 2297–2300. http://dx.doi.org/10.1029/2001GL012869.
Saffer, D.M., Marone, C., 2003. Comparison of smectite-and illite-rich gouge frictional properties: application to the updip limit of the seismogenic zone along subduction megathrusts. Earth Planet. Sci. Lett. 215, 219–235.
Sagi, D.A., 2012. Characterisation of the 2D and 3D Density and Connectivity Attributes of Fracture Systems in Carbonate Reservoir Analogues: Implications for Fluid Flow (Ph.D. thesis). University of Durham, UK.
Schleicher, A., van der Pluijm, B., Warr, L., 2010. Nanocoatings of clay and creep of the San Andreas Fault at Parkfield, California. Geology 38, 667–670.
Scholz, C.H., 1998. Earthquakes and friction laws. Nature 391, 37–42.
Sharp, Z., Papike, J., Durakiewicz, T., 2003. The effect of thermal decarbonation on stable isotope compositions of carbonates. Am. Mineral. 88, 87–92.
Shipton, Z.K., Soden, A.M., Kirkpatrick, J.D., Bright, A.M., Lunn, R.J., 2006. How thick is a fault? Fault displacement–thickness scaling revisited. Geophys. Monogr. Ser. 170, 193–198.
Shoval, S., 2003. Using FT-IR spectroscopy for study of calcareous ancient ceramics. Optic. Mater. 24, 117–122.
Sibson, R., 1977. Fault rocks and fault mechanisms. J. Geol. Soc. 133, 191–213.
Sibson, R.H., 1989. Earthquake faulting as a structural process. J. Struct. Geol. 11, 1–14.
Sibson, R.H., 2003. Thickness of the seismic slip zone. Bull. Seismol. Soc. Am. 93, 1169–1178.
Smith, S.A.F., Billi, A., Toro, G.D., Spiess, R., 2011a. Principal slip zones in limestone: microstructural characterization and implications for the seismic cycle (Tre Monti Fault, Central Apennines, Italy). Pure Appl. Geophys. 168, 2365–2393.
Smith, S.A.F., Holdsworth, R.E., Collettini, C., Pearce, M.A., 2011b. The microstructural character and mechanical significance of fault rocks associated with a continental low-angle normal fault: the Zuccale fault, Elba Island, Italy. Geol. Soc., Lond., Spec. Publ. 359, 97–113.
Smith, S., Di Toro, G., Kim, S., Ree, J.H., Nielsen, S., Billi, A., Spiess, R., 2013. Coseismic recrystallization during shallow earthquake slip. Geology 41, 63–66.
Sone, H., Shimamoto, T., Moore, D.E., 2012. Frictional properties of saponite-rich gouge from a serpentinite-bearing fault zone along the Gokasho-Arashima Tectonic Line, central Japan. J. Struct. Geol. 38, 172–182.
Tembe, S., Lockner, D.A., Wong, T.F., 2010. Effect of clay content and mineralogy on frictional sliding behavior of simulated gouges: binary and ternary mixtures of quartz, illite, and montmorillonite. J. Geophys. Res. 115, B03416. http://dx.doi.org/10.1029/2009JB006383.
Tesei, T., Collettini, C., Carpenter, B.M., Viti, C., Marone, C., 2012. Frictional strength and healing behavior of phyllosilicate-rich faults. J. Geophys. Res. 117, B09402. http://dx.doi.org/10.1029/2012JB009204.
Tesei, T., Collettini, C., Viti, C., Barchi, M.R., 2013. Fault architecture and deformation mechanisms in exhumed analogues of seismogenic carbonate-bearing thrusts. J. Struct. Geol. 55, 167–181.
Trabucho-Alexandre, J., Negri, A., de Boer, P.L., 2011. Early Turonian pelagic sedimentation at Moria (Umbria–Marche, Italy): primary and diagenetic controls on lithological oscillations. Palaeogeogr. Palaeoclimatol. Palaeoecol. 311, 200–214.
Verberne, B.A., He, C., Spiers, C.J., 2010. Frictional properties of sedimentary rocks and natural fault gouge from the Longmen Shan fault zone, Sichuan, China. Bull. Seismol. Soc. Am. 100, 2767–2790.
Walker, R.J., Holdsworth, R.E., Armitage, P.J., Faulkner, D.R., 2013. Fault zone permeability structure evolution in basalts. Geology 41, 59–62.
Wangen, M., 2010. Physical Principles of Sedimentary Basin Analysis. Cambridge University Press, Cambridge.
Westaway, R., Gawthorpe, R., Tozzi, M., 1989. Seismological and field observations of the 1984 Lazio-Abruzzo earthquakes: implications for the active tectonics of Italy. Geophys. J. Int. 98, 489–514.
Wibberley, C.A.J., Shimamoto, T., 2003. Internal structure and permeability of major strike-slip fault zones: the Median Tectonic Line in Mie Prefecture, Southwest Japan. J. Struct. Geol. 25, 59–78.
Wilkinson, M., McCaffrey, K., Roberts, G., Cowie, P., Phillips, R., Michetti, A.M., Vittori, E., Guerrieri, L., Blumetti, A., Bubeck, A., 2010. Partitioned postseismic deformation associated with the 2009 Mw 6.3 L'Aquila earthquake surface rupture measured using a terrestrial laser scanner. Geophys. Res. Lett. 37, L10309. http://dx.doi.org/10.1029/2010GL043099.
Woodcock, N., Mort, K., 2008. Classification of fault breccias and related fault rocks. Geol. Mag. 145, 435–440.
Yasuhara, H., Marone, C., Elsworth, D., 2005. Fault zone restrengthening and frictional healing: the role of pressure solution. J. Geophys. Res. 110, B06310. http://dx.doi.org/10.1029/2004JB003327.
Zoback, M., Hickman, S., Ellsworth, W., 2010. Scientific drilling into the San Andreas Fault zone. Eos, Trans. Am. Geophys. Union 91, 197–199.